Single cell transcriptomics of ferrets reveal a common temporal pattern of progenitors in brain development of gyrencephalic mammals

Authors list

Merve Bilgic[1, 2, 3], Quan Wu[1*], Taeko Suetsugu[1], Yuji Tsunekawa[1,4], Atsunori Sitamukai[1],Mitsutaka Kadota[5], Osamu Nishimura[5], Shigehiro Kuraku[5,6], and Fumio Matsuzaki[1, 2, *]

Affiliations

[1]Laboratory for Cell Asymmetry, RIKEN Center for Biosystems Dynamics Research, Kobe, Hyogo 650-0047, Japan.

[2]Laboratory of Molecular Cell Biology and Development, Department of Animal Development and Physiology, Graduate School for Biostudies, Kyoto University, Kyoto 606-8501, Japan.

[3]Present address: The Institute for Quantitative Biosciences, The University of Tokyo, Tokyo 113-0033, Japan.

[4]Present address: Division of Molecular and Medical Genetics, Center for Gene and Cell Therapy, The Institute for Medical Science, The University of Tokyo, Tokyo 108-0071, Japan.

[5]Laboratory for Phyloinformatics, RIKEN Center for Biosystems Dynamics Research, Kobe, Hyogo 650-0047, Japan.

[6]Present address: Molecular Life History Laboratory, Department of Genomics and Evolutionary Biology, National Institute of Genetics, Mishima, Shizuoka 411-8540, Japan.

[*]Corresponding authors

quan.wu@riken.jp

fumio.matsuzaki@riken.jp

Further information and requests for resources and reagents should be directed to and will be fulfilled by the lead contact, Fumio Matsuzaki (fumio.matsuzaki@riken.jp)

SUMMARY

The diversity of neural stem cells is a hallmark of gyrencephalic brains, including that in humans. Ferrets are an excellent model to study the complex brain development in gyrencephalic mammals, but information on their neural progenitor subtypes is fragmentary. Here, we investigated the temporal series of single-cell transcriptomes of progenitors in developing cortices in ferrets for comparison with human datasets. We found that the diversity and temporal trajectory of neural progenitors, termed radial glia (RG), are well conserved between ferrets and humans. Truncated RG (tRG), a progenitor subtype previously described in humans, and outer RG-like cells were assigned to ferret transcriptomes. *In vivo* and transcriptome analyses indicated that ferret tRG are generated via asymmetric RG divisions during late neurogenesis, and suggested that tRG is eventually fated to ependymal and glial populations. Therefore, the combined analyses of human and ferret transcriptomes enable the determination of progenitor fate sequences *in vivo*.

Keywords:

Single-cell transcriptome, neural stem cell, brain development, ferret, human, neurogenesis, truncated radial glia

INTRODUCTION

A vast diversity of neurons and glia form functional neural circuits during the development of the cerebral cortex to dictate its elaborated tasks in mammals. These cells are progressively derived from multipotent neural stem cells, called radial glia (RG), which generate neurons of the deep layers (DL) and upper layers (UL), and subsequently undergo gliogenesis to generate astrocytes and/or oligodendrocytes (Figure 1A, Rowitch and Kriegstein, 2010). During this process, RG division at the ventricular zone (VZ) generates terminally differentiated cells or intermediate progenitor cells (IPC) that are mitotically active to generate differentiated cells in the VZ or sub-VZ (SVZ). Therefore, the spatiotemporal patterns of neural progenitor cells (NPC), including RG and IPC, are crucial for constructing the functional architecture of six neuronal layers in the cerebral cortex (Rossi et al., 2017).

The cerebral cortex has undergone great expansion during mammalian evolution, often leading to surface folding. One of the crucial factors is the SVZ expansion, specifically the emergence of a new germinal layer, the outer SVZ (OSVZ), during cortical development (Smart et al., 2002). The OSVZ contains outer RG (oRG) cells (Hansen et al., 2010; Fietz et al., 2010) which

contribute to the amplification of neuronal and glial outputs in the cortex (Figure 1A; Rash et al., 2019). Unlike lissencephalic species, the OSVZ grows significantly in gyrencephalic species, including primates and carnivores such as ferrets (Shitamukai et al., 2011; Wang et al., 2011; Hansen et al., 2010; Fietz et al., 2010; Reillo et al., 2011). In contrast to bipolar RG cells in the VZ (vRG), oRG cells are unipolar and have a basal fiber connected to the pial surface without an apical endfoot (Figure 1A; Fietz et al., 2010; Hansen et al., 2010). A new subtype of NPC in the VZ has been reported in humans and rhesus macaques (Figure 1A; Nowakowski et al., 2016, deAzevedo et al., 2003; Sidman and Rakic, 1973), lacking the basal attachment and is therefore termed truncated RG (tRG). However, whether tRG is formed in a wide range of gyrencephalic mammals, mechanisms underlying their formation, and their descendants remain unknown. As distinct subtypes of NPC possess different capacities to generate neuronal and glial progenies (Rash et al., 2019; Huang and Bhaduri et al., 2020), characterizing their molecular and cellular properties, mutual relationships during development, and terminal types of cells they produce are crucial factors.

Genetic manipulation of individual cell types *in vivo* and single-cell transcriptome analysis are two major and successful approaches in revealing the properties of cells, such as their proliferation and differentiation. Single-cell RNA sequencing (scRNA-seq) of the human brain during development has been extensively performed (Pollen and Nowakowski et al., 2015; Johnson, Wang and Atabay et al., 2015; Liu et al., 2017; Nowakowski et al., 2017; Zhong and Zhang et al., 2018; Polioudakis et al., 2019; Bhaduri et al., 2020; Huang et al., 2020; Bhaduri and Sandoval-Espinosa et al., 2021). However, *in vivo* behavior of human NPC and the underlying mechanisms remain less explored owing to limited experimental access of the developing human cortex. Particularly, resources available for the late human embryonic brain are extremely rare. Studies using brain organoids face issues in recapitulating the specification and maturation of cell types during human brain development (Bhaduri et al., 2020). In this context, the ferret (*Mustela putorius furo*) is highlighted as a suitable animal model to compensate for the difficulties in studying human cortical development. The ferret is a carnivore that develops common gyrencephalic features, such as the OSVZ and a folded brain, and is experimentally available for *in vivo* gene manipulation and editing using *in utero* electroporation (IUE; Kawasaki et al., 2012, Matsui et al., 2013, Tsunekawa et al., 2016). Severe microcephalic phenotypes in *Aspm* (*Abnormal Spindle-like Microcephaly-associated*) knockout ferrets with a similar degree to human cases have suggested the use of ferrets for studying neurodevelopment and disorders of gyrencephalic species (Johnson et al., 2018; Kou

and Wu et al., 2015), in contrast to a minor phenotype in mouse *Aspm* mutants (Pulvers et al., 2010; Fujimori et al., 2014; Capecchi et al., 2015; Jayaraman et al., 2016). Transcriptome profiling of ferret cortical cells has been performed to reveal regional distinctions in germinal layers and cell-type composition (de Juan Romera et al., 2015; Johnson et al. 2018). However, the temporal pattern of molecular signatures of ferret NPC remains largely unexplored at single-cell resolution. Comparison of progenitor subtypes and sequential events at single-cell transcriptome levels along the developmental course in ferrets and between the ferrets and humans will greatly help to recognize common and species-specific mechanisms underlying the construction of the complex brain.

In this study, we aimed to comprehensively analyze the developmental dynamics of ferret progenitor populations both *in vivo* and *in silico* to compare the cortical development between ferrets and humans at molecular and cellular levels. Transcriptome profiles of ferret cortical cells were analyzed from different developmental stages that cover the early to-late neurogenic and gliogenic phases and diverse cell types were identified. The resultant ferret dataset and published human datasets were integrated for a cross-species comparison that led us to assign tRG- and oRG-like cells as transcriptionally distinct subpopulations in ferrets. Furthermore, the combination of *in silico* comparison between ferrets and humans and *in vivo* analysis in ferrets aided in determining the mode of tRG generation from RG and the fate of their descendants. The results will promote our understanding of the roles of diverse NPCs in gyrencephalic animals, emphasizing the values of the current single-cell ferret transcriptomes.

RESULTS

Temporal patterns of neurogenesis and gliogenesis in ferret cerebral cortex

To visualize the course of neurogenesis and gliogenesis in the developing ferret brain, we performed immunohistochemistry of the somatosensory cortex at embryonic days E25, E32, E36, and E40, and postnatal days P5 and P10, covering the developmental events (Figure 1B). We explored the distribution of RG, IPC, and oligodendrocyte precursors (OPC) by co-staining for their markers (PAX6, TBR2, and OLIG2, respectively, Figure 1B-G), and the distribution of astrocytes and their progenitor cells by staining for glial fibrillary acidic protein (GFAP; Figure S1B). The $PAX6^+$ RG and $TBR2^+$ IPC were virtually confined to the VZ and SVZ, respectively, until E32 (Figure 1B, C). Neurogenesis already commenced at E25 (Figure S1A; Poluch et al., 2015) and resulted in an enlargement of the $TBR2^+$ IPC-containing SVZ and

expansion of the cortical plate (CP) by E32 (Figure 1C). We confirmed the temporal pattern of neuronal layer formation in the somatosensory cortex using two markers, CTIP2 (layer V; Arlotta et al., 2005) and SATB2 (an upper-layer marker; Szemes M *et al*, 2006; Britanova and Akopov *et al*., 2005; Figure S1A). During E32, a layer V/VI ($CTIP2^+$) was generated (McConnell, 1988; Noctor et al., 1997). At E36, $SATB2^+$ neurons were detectable on both the deeper and upper sides of the $CTIP2^+$ layer, suggesting the generation and migration of $SATB2^+$ upper-layer neurons by E36. Subsequently, $GFAP^+$ RG with gliogenic potential emerged by E40, whereas $GFAP^+$ maturating astrocytes with a typical astrocytic morphology appeared outside the germinal layers at a much later stage around P5 onward (Figure S1B; Reillo et al., 2012). The $PAX6^+$ progenitors started dispersing outside the VZ along the entire cortex around E32 (Figure 1C), and then formed an OSVZ harboring oRG multipotent progenitors by E36 (Figure 1D; Fietz et al., 2010; Reillo et al., 2011; Poluch et al., 2015). The parietal OSVZ expanded the most around birth (Figure 1E) and gradually diminished by P10 (Figure 1F, G). OPCs are derived from RG on the ventral side and the dorsal RG in both mice (Zheng et al., 2018) and humans (Rash et al., 2019; Huang et al., 2020; Kessaris and Fogarty et al., 2006). We confirmed a similar phenomenon in ferrets (Figure S1C, see also STAR Methods).

Single-cell RNA-seq reveals signatures of gene expression and subtypes of ferret cortical cells

Despite several transcriptome studies on the ferret cortex (de Juan Romera et al., 2015; Johnson et al., 2018), incomplete information on the ferret genome (specifically, poor information of the 3'-untranslated region (UTR) of genes) has interfered with single-cell transcriptome analysis at a high resolution. We improved the quality of ferret genomic annotation and constructed new gene models using Chromium by tagging all fragments from a long genomic DNA in a droplet (Table S1; STAR Methods). We then applied 10X Genomics scRNA-seq technology to analyze the molecular signatures of neural progenitor subtypes covering early-to-late neurogenesis and gliogenesis (E25, E34, E40, P1, P5, P10). Cell populations were isolated by two ways to enrich the progenitor subtypes (Figure 2A): (1) FACS-based sorting of fluorescent cells from tissues that had been electroporated at E30 or E34 with AzamiGreen (AG) expression vector (Karasawa et. al. 2003) under the control of *Hes5* promoter with a d2 degradation signal (STAR Methods; Ohtsuka et al. 2006) and (2) collecting cells from the VZ,

SVZ, and intermediate zones (IZ, Figure 2A) of the cerebral cortex after discarding the CP to decrease the abundance of mature neurons. These two cell populations were combined for downstream analyses (STAR Methods). Unbiased clustering was employed based on the shared nearest neighbors and projected cells in the Uniform Manifold Approximation and Projection (UMAP) space using Seurat package (Figure 2B, C, Stuart and Butler et al., 2019). After removing low-quality cells, we characterized 26 transcriptionally distinct clusters from 30,234 ferret cortical cells at different stages and detected up to 2600 median genes per cell (Figure S2A, B; Table S1). Cell clusters were annotated according to their specific gene expression patterns (Figure 2D, E, S2D, Table S1) and assigned 10 cell types: RG (early, mid, and late), IPC, OPC, ependymal cells, excitatory cortical neurons (DL and UL), inhibitory neurons (ITN), microglia, endothelial cells, mural cells, and a population of unknown cells (Figure 2D, E). Early and late RG, and IPC were subdivided into three subclusters that expressed different cell cycle markers (Figure S2C).

We assigned the early and late RG clusters by their collection stages and the expression of temporally altered RG markers (hereafter temporal markers) previously reported (*Hmga2, Ldha,* and *Lix1* for early RG, and *Ptn, Aldoc,* and *Fabp7* for late RG; Okamoto et al., 2016) as shown in Figure 2D (see Figure S2D and Table S2). The "early RG" clusters comprised E25 cells; "mid RG" clusters, mostly of E34 cells, and "late RG" groups, with cells from E34 and later stages (Figure S2E). Therefore, RG clusters were distinguished according to their sequential transcriptional profiles rather than a sample batch. RG clusters (expressing *Vim*, *Pax6*, and *Hes5*), IPC (expressing *Eomes*, *Neurod4*, and *Hes6*), and neuronal clusters (expressing *Stmn2* and *Neurod6*) were aligned according to the neuronal differentiation process in the UMAP plot (Figure 2C). These changes in the transcriptional profiles of RG along the temporal and differentiation axes were consistent with the *in vivo* development.

Interestingly, we identified a small cluster (409 cells) of *Pax6*-expressing RG subtype, 69% of which expressed *Cryab* (Figure 2F). *Cryab*, encoding a molecular chaperone (Yamamoto et al., 2014), is a unique marker for human tRG (Figure 2F; Nowakowski et al., 2016); therefore, we designated them as tRG-like cells in ferrets. In contrast, oRG cells were not identified as distinct clusters from vRG cells in ferrets by unbiased clustering (Figure 2B, G). A typical *in vivo* example is that HOPX, a good marker for oRG in human tissues (Pollen et al., 2015). is expressed in both oRG and vRG (Figure 2H; Kawaue et al., 2019; Johnson et al., 2018).

The radial-glia subtypes in ferrets correlate with their human counterparts

Both ferrets and humans represent complex brain features of gyrencephalic mammals and are located in distinct phylogenic branches. Therefore, comparing RG subtypes and their temporal patterns of birth, transitions, and differentiation is beneficial to distinguish the developmental processes specific to a particular species or common for complex brain formation. We successfully compared them at the single-cell transcriptome level using our ferret dataset and a previously published human dataset (Nowakowski *et al*., 2017).

We used a published package (Seurat) to integrate the ferret dataset with human dataset, including all types of cells obtained from the somatosensory cortex. The two datasets were merged using pairs of cells with the most similar biological states. Each pair containing one human and one ferret cell, was identified by the mutual nearest neighbors (MNNs) after Canonical Correlation Analysis (CCA) of two datasets (Stuart and Butler et al., 2019; See STAR Methods).

This computation revealed that various cell types, including RG, IPC, OPC, neurons, mural cells, endothelial cells, and microglial cells, were clustered together across datasets (Figure 3A, S3A). The cell-type composition from both species was similar across ages; on the UMAP plot, ferret E25 cells were closely distributed with their counterparts human GW8; ferret E34 with human GW11-14; ferret E40-P1 with human GW15-16, and ferret P5-P10 with human GW17-22 (Figure 3B), suggesting that these pairs corresponded to each other. Consistently with our *in vivo* observations in ferrets (Figure 1, S1), gliogenic RG cells (a subtype of "late_RG" group and OPC in Figure 2B) were first distinguished transcriptionally at E40 in the ferret and at GW14 in human datasets (arrowheads in Figure 3B).

Next, we compared the similarities among RG subtypes in humans and ferrets. To quantify the features of an RG subtype, we introduced a parameter, marker-gene score (Bhaduri et al., 2020), which is used to describe the expression pattern (degree of abundance and specificity) of a marker gene in a given cluster; the score for a marker gene is defined by multiplying the average enrichment of expression level in the cluster (fold change) and the ratio of the number of cells expressing the marker in the cluster to that in all other clusters (see STAR Methods). We hypothesized that if two cell clusters from two different species belong to the same cell type, they should share similar marker genes and each marker gene should have a similar score. We evaluated the correlation between two arbitrary RG subtypes from humans and ferrets by calculating the marker-gene scores for a set of cluster marker genes, the expression of which was shared by the pair of RG subtypes of interest (Table S2).The early and late RG clusters

were found to be related across species with a significantly high similarity (Figure 3C, D); the early RG clusters in ferrets were highly correlated with those of humans, and the late RG clusters in ferrets were similar to human vRG, oRG, and tRG. The correlation of the transcriptome profile between ferret tRG-like cells and human tRG was significantly high. Ferret tRG-like clusters and human tRG clusters expressed *Cryab*, *Egr1*, *Cyr61,* and *Sparc* at higher levels than did the other RG clusters (Figure 3E), confirming that these genes are the global tRG markers shared by ferrets and humans.

Marker gene scores can also be used to determine the correlation between cell clusters of two species (e.g., ferrets and humans) based on the assumption that cells belonging to a specific subtype should highly and specifically express the marker genes. Therefore, we defined the cluster score for a cell as a linear combination of the expression level of each marker gene in the cell weighted by its marker-gene score in the human cluster of interest. We separately calculated the tRG score for all RG cells in the ferret and human datasets. Expectedly, tRG-like cells had a significantly higher tRG cluster score than any other cluster in the ferret and human datasets (Figure 3F). Considering that the tRG score for ferret cells was calculated using marker-gene scores of the human tRG cluster, we concluded that tRG-like cells in ferrets share transcriptomic profiles similar with human tRG cells.

tRG emerge around birth during the development of somatosensory cortex in ferrets

Finding tRG-like clusters in ferret transcriptome suggests the presence of RG-like cells with short fibers in the ferret cortex at late neurogenic stages, which is similar to the human brain. We then investigated how and when such RG cells emerged in developing cortical tissues of ferrets. To visualize tRG-like cell morphology, we sparsely electroporated late-embryonic and newborn ferrets with an expression vector for enhanced green fluorescent protein (EGFP, see STAR Methods). EGFP labeling at P0 revealed RG cells with a truncated basal fiber and apical endfoot (Figure 4A), as previously reported in human tissues (Nowakowski et al., 2016).

tRG cells emerge and express CRYAB during late neurogenic and early gliogenic stages (Nowakowski et al., 2016). Similarly, in ferret tRG-like cells *in vivo,* CRYAB expression emerged shortly prior to birth, at the late neurogenic and early gliogenic stages (Figure S4F) and became mostly restricted to tRG-shaped cells in the VZ and SVZ (Figure 4B, S4B-D). These cells increased in number by P10 (Figure 4C). These histochemical observations were in accordance with our transcriptome data; the population of ferret tRG-like cells increased

during late development (Figure 4D) with the majority becoming *Cryab*$^{+}$ (Figure S4E). Meanwhile, only 5% of RG at the late stage expressed *Cryab* (Figure S4C). We further analyzed the *in vivo* cellular properties of tRG by staining with cell fate markers from the late neurogenic stage onward. The majority of CRYAB^{+} cells in the VZ and SVZ expressed low levels of TBR2, OLIG2, and KI67 at P5 and P10 (Figure 4E-G and 4E'–G'), suggesting that these cells were mostly post-mitotic (KI67^{-}) and neither IPC (TBR2^{+}) nor OPC (OLIG2^{+}) at P10. These histochemical data were again consistent with our single-cell transcriptome data (Figure S4G). Concomitantly, the Gene Ontology (GO) term analysis of the ferret tRG cluster showed gene expression related to negative regulation of neurogenesis, neuron differentiation, and extracellular matrix organization (Figure S4H). Therefore, tRG-like cells in ferrets are equivalent to human tRG cells, and are further defined as tRG cells in ferrets. We noted a difference between humans and ferrets; conventional RG cells extending a radial fiber to the laminar surface also coexisted with these tRG cells in the VZ during postnatal development (Figure S4A), whereas the VZ became completely separated from the OSVZ in the corresponding stages of the human cortex as conventional RG cells were absent in the VZ (Nowakowski et al., 2016).

tRG are formed from the apical division of RG sibling cells with a short basal fiber

As predicted by pseudo-time trajectory analysis (Figure 5), tRG cells most likely originate from the late RG population. However, single-cell transcriptome analysis does not tell us how tRG are formed from the late RG, directly from RG by shortening their basal fiber, as a sibling from asymmetric divisions of RG cells, or more indirectly as progeny cells through further divisions of RG sibling cells. We addressed this question using time-lapse imaging of cortical slices of ferrets. To follow the sequential pattern of cell divisions and the shape of progeny cells in RG lineages, we introduced an EGFP-expressing vector using IUE at E35. 5-Ethynyl-2'-deoxyuridine (EdU) labeling as early as E38 detected cells in the ependymal layer, the final destination of majority of tRG cells (Figure S4I, and see the next section). Based on this observation, we started time-lapse imaging of slices in culture at E38 or P0, and continued imaging for three days, then fixed and stained slices for CRYAB and EGFP (STAR Methods). Using this procedure, we reconstructed the process of tRG formation from mitotic progenitor cells (four examples); in all these cases, vRG cells were not directly differentiated into tRG. Instead, CRYAB^{+} cells were produced as daughter cells of an apical division of mitotic progenitor cells that bore both an apical endfoot and a short basal fiber (the deep blue cell in

Figure 4H). These non-vRG progenitor cells (the deep blue cell in Figure 4I) underwent interkinetic nuclear migration within the VZ and asymmetrically divided (13:20 in Figure 4H) into a CRYAB$^+$ daughter without the short fiber (the deep blue cell 13:20 onward in Figure 4H) and a non-CRYAB-expressing daughter that inherited the short basal fiber (the light blue cell), as schematically drawn in Figure 4I. This CRYAB$^+$ cell extended a short basal process to acquire the tRG form (14:00–60:00 in Figure 4H, J). In two of these four examples, the mitotic mother cells of tRG (the deep blue cell in Figure 4K, L, see Supplementary movie 1) were generated as the sibling cells of a dividing vRG with a full-length radial fiber (the pink cell during 0:00–40:00 in Figure 4K, M). In the other two cases, we could not follow the birth of the tRG mother cell because of technical issues. Altogether, our data suggest that tRG cells are formed by apical asymmetric division(s) of unique apical IPCs with a short basal fiber (Tsunekawa et al. in preparation). We note the possibility that these IPC, which asymmetrically generated tRG, already expressed CRYAB. Indeed, a certain portion of CRYAB-expressing tRG (approximately 20%) was mitotically active, whereas it was post-mitotically declined (Figure 4E).

Temporal fates of RG cells are predicted by pseudo-time trajectory analysis

To understand the relationship between various cortical progenitors in the developing ferret brain, particularly the origin and fate of ferret tRG, pseudo-time trajectory analysis was performed using Monocle 2 (Trapnell and Cacchiarelli et al., 2014; Qiu and Mao et al., 2017). All single cells that had been subjected to single-cell transcriptome analyses (from E25 to P10) were unbiasedly ordered along a trajectory (Figure S5A, B) based on their transcriptome profiles. To simplify our analysis, we first excluded interneurons, microglia, endothelial cells, and excitatory neuronal clusters. Subsequently, 6,000 single cells were randomly selected from the remaining cell population for further analysis (see STAR Methods). We confirmed that this procedure successfully predicted the developmental trajectory of the somatosensory area, along which the selected cells were arranged in order from the earlier to later stages (Figure 5B). The pseudo-time analysis predicted a reasonable trajectory consisting of three branching points that generated seven branches (Figure 5A, S5B). We assigned major cell types for each branch on the basis of cell clusters defined by UMAP analysis (Figure 2, 5C, S5D; Table S3), naming each branch after its dominant cell type (Figure 5A); the first branching point generated the neuronally differentiated lineage (branch 2) and NPC 2 (branch 3); the second branching produced the OPC lineage (branch 4) and NPC 3 (branch 5); and the final branching point generated the ependymal (branch 6) and astroglial lineages (branch 7). This trajectory began

with progenitor cells from early embryonic stages (E25; Figure 5B), and RG cells between E34 and P1 gave rise to both neurogenic and gliogenic trajectories (Figure 5B, S5C, D). After birth, neurogenesis gradually declined, whereas gliogenic processes progressed (Figure 5B). The distribution of marker gene expression, and clusters along the pseudo-time trajectories suggested that the final branching segregated the NPC type3 cells (*Ptn*) into ependymal (*Foxj1*) and astroglial (*Aqp4*) fates (Figure 5C, S5C-D).

tRG cells possess ependymal and gliogenic potential during cortical development of ferrets

Interestingly, tRG cell population was distributed into three branches along the trajectory in the pseudo-time trajectory analysis (Figure 5D); NPC type3 (mainly during E40-P1), astroglial (from P1-P10), and ependymal (from P5-P10; Figure 5E) branches. Therefore, tRG prenatally arose as precursors of ependyma and astroglia in the ferret cortex. To test this hypothesis, we first examined cells differentiating into ependymal cells by immunostaining for a typical ependymal marker, FOXJ1, a master regulator of ciliogenesis, along with staining for CRYAB. We observed that $CRYAB^+$ tRG cells gradually co-expressed FOXJ1, reaching up to 90% of $CRYAB^+$ cells to be $FOXJ1^+$ by P10 (Figure 6A, B). Similarly, our transcriptome data showed that the fraction of *Cryab-Foxj1* double-positive cells increased in the tRG cluster from P1 to P10, whereas other RG clusters maintained low *Cryab* expression (Figure 6C, D). We further confirmed that differentiating ependymal cells resided within the VZ from P5 onwards (Figure 6A). These cells possessed short basal fibers with a cell body that finally settled on the apical surface by P14 (Figure 6E). These data suggest that some tRG cells progressively upregulate *Foxj1* expression to adopt an ependymal cell fate during post-natal development. Concomitantly, detectable ADENINE CYCLASE III expression in both primary and multi-cilia cells indicated that ciliogenesis progressed postnatally, forming multi-ciliated ependymal cells on the ventricular surface of the ferret cortex by P35 (Figure 6F).

Transcriptional analysis of human tRG subtypes by integration with ferret tRG subtypes

We then performed transcriptome analysis to assess whether human tRG cells possess ependymal and gliogenic potential, as observed in ferrets. We tried to upgrade the resolution of our analysis considering two points: (1) choosing a recently published human dataset, which

include cells at GW25 and more tRG cells than do the previous datasets (Bhaduri et al., 2021), and (2) focusing our comparison on NPC populations, excluding neurons and other cell types from analysis. This approach identified respective clusters for tRG and oRG cells based on shared nearest neighbor clustering using their marker gene expression (Figure 7A and Table S4). We then merged human and ferret NPCs based on CCA-MNN (Figure 7B, C), a strategy described before (Figure 3A). The correlation between two arbitrary RG subtypes from humans and ferrets, which was calculated from marker-gene scores for the set of cluster marker genes, indicated that tRG and oRG in humans shared similar transcriptomes with tRG and later RG in ferrets, respectively (Figure S6A, B). We note that early RG in ferrets showed the highest similarity with "OLIG1" in human data, and no cell type in human data corresponded to ferret "midRG", likely because only GW25 cells were chosen for comparison (see Figure S6B legend).

The integration of ferret and human datasets, as described above, showed that human and ferret tRG were mainly distributed into three different clusters: 7, 21, and 28 (Figure S6C, 7D, F). Cells in cluster 7 shared a transcriptomic expression pattern similar to that of the late RG cells, which was characterized by high expression of RG marker genes (such as *APOE*, *FABP7*, *NOTCH2*, and *DBI*; Figure S6D). Therefore, tRG cells in cluster 7 were in a late RG-like state that was presumably uncommitted to astroglial or ependymal fates (corresponding to cells in the NPC 3 branch in the pseudo-time trajectory; Figure 5A). In contrast, cells in clusters 21 and 28 highly expressed marker genes as observed in the astrocyte (GFAP and AQP4) and the ependymal (FOXJ1 and CRYAB) clusters, respectively (Figure S6D and Table S4). To validate this classification of tRG cells into three main clusters after integration, we compared the clustering of ferret tRG cells in the merged dataset with the classification of ferret tRG cells in the pseudo-time trajectory analysis (Figure 7G). Indeed, these two independent approaches largely produced consistent results for classifying ferret tRG cells, suggesting that the bifurcation of tRG fates was reliable; for example, most tRG cells in the astroglia branch were assigned to cluster 21 (characterized by a strong expression of astrocyte markers) in the integrated dataset (Figure 7G). As human and ferret tRG cells shared a similar clustering result in the merged dataset, our results suggested that tRG cells in both humans and ferrets possessed the potential to generate astrocytes and ependymal cells. The proportion of the three types of tRG was different between human and ferret datasets, in which increased ependymal and gliogenic tRG cells were observed in ferrets and elevated late RG-like tRG cells were observed

in the human GW25 dataset (Figure 7D-F). This difference may be ascribed to the difference in developmental stages between the two datasets (see Discussion).

Prediction of oRG-like cells using human anchors

oRG could not be identified as a separate cluster in the ferret dataset. Attempts were made to assign oRG-like cells in the ferret dataset using human oRG cells as anchors, as was done for the tRG subtypes. During the integration of two datasets using Seurat, we already identified the MNN after CCA of both datasets, which made a nearest neighbor-pair between a ferret and a human cell, as described before (Figure 7B). These two cells had the most similar transcriptome profiles compared with other cells in each dataset, suggesting that the ferret cell which paired with a human oRG can be assigned as a ferret oRG-like cell. The assigned oRG-like ferret cells were located near the human oRG cluster (Figure 7H). To assess the degree of similarity to human oRG, we calculated the oRG score for each ferret oRG-like cell (Figure 3E). The oRG-like cells assigned by MNN had significantly higher oRG cluster score than that of all other NPCs (Figure 7I). Because the cluster score successfully distinguished tRG cells from other cell types (Figure 3), we hypothesized that these oRG-like cells would show a transcriptome profile similar to that of authentic oRG in ferrets. A comparison between oRG-like cells and other NPCs in the ferret dataset identified genes that were highly expressed in oRG-like cells (Table S4). Consistent with the human dataset (Bhaduri et al., 2021), the expression of HOPX, CLU, and CRYM was higher in oRG-like cells than in other NPCs (Figure 7J, S6E). However, investigation in ferrets using *in situ* hybridization showed that typical human oRG markers, such as HOPX and CLU, were expressed in vRG and tRG as well as oRG (Figure S6F). Therefore, in ferrets, oRG can only be distinguished by a combination of several markers or the whole transcriptome, instead of a few marker genes.

DISCUSSION

In this study, a dataset of single-cell transcriptomes was generated using an improved gene model, which showed the developmental sequences and diversity of neural progenitor populations during ferret cortical development. This dataset allowed us to compare the progenitor subtypes and temporal patterns of their appearance between humans and ferrets at a high resolution, using the accumulated information of human embryonic cortical single-cell transcriptomes (Nowakowski et al., 2016, Bhaduri et al. 2020, Bhaduri et al., 2021). We found that ferrets (carnivora) and humans (primates), representing two different orders of gyrencephalic animals, shared a large proportion of progenitor variations and their temporal

sequences despite their extremely different temporal scales of neural development. This work emphasizes the importance of ferrets as a model animal to study the neural development of gyrencephalic animals. Information regarding the revised gene model is publicly available to help in accelerating comparative studies and gene modification approaches using ferrets.

Temporal pattern of ferret progenitors

The temporal pattern and variation in ferret NPC were typically represented by a pseudo-time lineage trajectory and confirmed by immunohistochemical analysis of the developing brains (Figure 1). In the pseudo-time trajectory, Hes1$^+$ NPC passes through three consecutive branching points, each of which produces a side branch fated into terminal differentiation (first neurons, second oligodendrocytes, and third ependymal cells). This result is consistent with a consensus for the temporal transitions of embryonic neural stem cells from neurogenic to gliogenic, and with a recent finding of oligodendrocyte formation in the human dorsal cortical primordium (Huang et al. 2020). These self-renewing Hes1$^+$ and side branches gradually changed transcription profiles as the pseudo-time increased, and multiple progenitor types coexisted in parallel. The latest differentiating branching in the trajectory during the analyzed period generated tRG (Nowakowski et al. 2016) that was committed to ependymal fates. However, the tRG are not the last progeny of Hes1$^+$ NPC in ferrets. Instead, the tRG branch is parallel to another Hes1$^+$ NPC, which are mostly astrocyte progenitors that include a tRG subtype fated into astrocytes.

The origin and fates of tRG revealed by live imaging and single cell transcriptomes

Live imaging of ferret brains indicated tRG generation via asymmetric divisions of RG-like progenitors with a short radial fiber. In ferrets, the production of this neurogenic type of progenitor from vRG was observed during earlier neurogenic stages (Tsunekawa et al. in preparation). These progenitors might change their fate to produce tRG during the late neurogenic and early gliogenic stages, contributing to gliogenesis and ependymal formation. As the sample size was small, further studies on this type of progenitor are needed.

While tRG were first identified in human brain development (Nowakowski et al. 2016), their detailed characteristics, such as the fate of their descendants, remain unclear. In ferrets, cells belonging to the tRG cluster are distributed into three interconnected branches: NPC3, ependymal (CRYAB$^+$, FOXJ1$^+$), and astrogenic (CRYAB$^+$, GFAP$^+$) branches in the pseudo-time trajectory. The tRG in the NPC3 branch were not committed to ependymal or astrogenic fates, suggesting that this tRG population was uncommitted. Histochemically, we confirmed

that a large part of the tRG became ependymal and astrogenic cells. This mode of ependymal cell formation is parallel to the bifurcation of ependymal cells and adult neural stem cells from the same progenitor population in the striatum on the ventral side (Ortiz-A'lvarez et al. 2019).

Our cross-species analysis using CCA-MNN combined with cluster score analysis predicted that human tRG were also classified into three classes with differential transcriptomes (Figure 7E), which corresponded to the three subtypes of ferret tRG. In GW25 human brains, the uncommitted tRG fraction appeared to be major unlike in ferrets, raising the possibility that human tRG at GW25 progresses less along the differentiation axis compared to ferret tRG at P5-P10, most of which are already committed to either ependymal or astroglial states. Human GW25 is almost the latest stages available, and samples at the later stages might be very difficult to obtain. However, the result from ferrets predicts that tRG adopt the fate of ependymal cells and astroglial cells at later stages. Thus, the cross-species analysis with ferrets and humans provides a prediction as an advantage in this case, although checking whether the prediction is correct in humans is preferable.

A remarkable difference in the spatio-temporal pattern of NPC between ferrets and humans is the coexistence of vRG and tRG in the VZ at ferret late neurogenic and gliogenic stages whereas tRG is almost major NPC in the VZ in humans, thereby resulting in the spatial separation of the VZ from the OSVZ where oRG reside at late neurogenic stages. Therefore, genes that are preferentially expressed in late RG (compared with other RG) such as HOPX and CLU show nearly exclusive expression in the OSVZ in human. In contrast, the expression of those genes are observed less differentially between the VZ and OSVZ because of their expression in vRG as well as tRG.

In summary, we performed a comprehensive single-cell analysis of ferret cortical progenitors over the entire neurogenic and early gliogenic periods, and demonstrated that cross-species comparisons greatly contribute to define NPC states transcriptionally. In addition, we highlighted similarities and differences in NPC variations and temporal patterns between two gyrencephalic mammals, ferrets and humans. We created a useful dataset of ferret transcriptomes and provided comparison protocols for single-cell transcriptome analysis with high resolution for two different stages, tissues, or species.

Acknowledgements

We thank Hiroshi Kiyonari for ferret breeding management; Kazuaki Yamaguchi, Rohab F. Abdelhamid, and Chiharu Tanegashima for sequencing of RNA and genomic DNA; Tomomi Shimogori for *in situ* hybridization; and all members of the Laboratory of Cell Asymmetry for technical supports and helpful discussion. This work was supported by JSPS KAKENHI Grant Numbers 18H04003, 17H05779, 19H04791, and RIKEN funds to F.M. M.B. was a RIKEN International Program Associate. Q.W. was supported by JSPS Postdoctoral Fellowship and RIKEN Special Postdoctoral Researcher Program.

Author contributions

F.M. and Q.W. supervised the project. M.B., Q.W., and F.M. designed experiments and wrote the manuscript. M.K., O.N., Q.W., Y.K., and S.K. constructed new ferret gene models. M.B. and Q.W. carried out scRNA-seq experiments and performed bioinformatics analysis. M.B., Y.T., A.S. and Q.W. performed molecular biological analysis. M.B. and T.S. performed histological analysis. T.S. carried out the time-lapse imaging. T.S. and Y.T. bred the ferrets.

Conflict of interest statement

The authors declare no competing interests.

Data and code availability statement

Genome assembly and Chromium linked-read sequences were deposited in the DDBJ under the accession number BLXN01000001-BLXN01022349 and DRA010274, and the gene models is available from Figshare under the DOI: 10.6084/m9.figshare.12807032. Single-cell RNA-seq data have been deposited in the DDBJ (PSUB013536).

Any information required to obtain and reanalyze the data reported in this paper is available from the lead contact upon request.

References

Arlotta, P., Molyneaux, B.J., Chen, J., Inoue, J., Kominami, R., and MacKlis, J.D. (2005). Neuronal subtype-specific genes that control corticospinal motor neuron development in vivo. Neuron *45*, 207–221.

Bhaduri, A., Andrews, M.G., Mancia Leon, W., Jung, D., Shin, D., Allen, D., Jung, D., Schmunk, G., Haeussler, M., Salma, J., et al. (2020). Cell stress in cortical organoids impairs molecular subtype specification. Nat. 2020 5787793 *578*, 142–148.

504 Bhaduri, A., Sandoval-Espinosa, C., Otero-Garcia, M., Oh, I., Yin, R., Eze, U.C., Nowakowski,
505 T.J., and Kriegstein, A.R. (2021). An atlas of cortical arealization identifies dynamic molecular
506 signatures. Nat. 2021 5987879 *598*, 200–204.
507 Britanova, O., Akopov, S., Lukyanov, S., Gruss, P., and Tarabykin, V. (2005). Novel
508 transcription factor Satb2 interacts with matrix attachment region DNA elements in a tissue-
509 specific manner and demonstrates cell-type-dependent expression in the developing mouse
510 CNS. Eur. J. Neurosci. *21*, 658–668.
511 Capecchi, M.R., and Pozner, A. (2015). ASPM regulates symmetric stem cell division by
512 tuning Cyclin E ubiquitination. Nat. Commun. 2015 61 *6*, 1–17.
513 DeAzevedo, L.C., Fallet, C., Moura-Neto, V., Daumas-Duport, C., Hedin-Pereira, C., and Lent,
514 R. (2003). Cortical radial glial cells in human fetuses: Depth-correlated transformation into
515 astrocytes. J. Neurobiol. *55*, 288–298.
516 Fietz, S.A., Kelava, I., Vogt, J., Wilsch-Bräuninger, M., Stenzel, D., Fish, J.L., Corbeil, D.,
517 Riehn, A., Distler, W., Nitsch, R., et al. (2010). OSVZ progenitors of human and ferret
518 neocortex are epithelial-like and expand by integrin signaling. Nat. Neurosci. *13*, 690–699.
519 Fujimori, A., Itoh, K., Goto, S., Hirakawa, H., Wang, B., Kokubo, T., Kito, S., Tsukamoto, S.,
520 and Fushiki, S. (2014). Disruption of Aspm causes microcephaly with abnormal neuronal
521 differentiation. Undefined *36*, 661–669.
522 Hansen, D. V., Lui, J.H., Parker, P.R.L., and Kriegstein, A.R. (2010). Neurogenic radial glia
523 in the outer subventricular zone of human neocortex. Nat. 2010 4647288 *464*, 554–561.
524 Huang, W., Bhaduri, A., Velmeshev, D., Wang, S., Wang, L., Rottkamp, C.A., Alvarez-Buylla,
525 A., Rowitch, D.H., and Kriegstein, A.R. (2020). Origins and Proliferative States of Human
526 Oligodendrocyte Precursor Cells. Cell *182*, 594-608.e11.
527 Jayaraman, D., Kodani, A., Gonzalez, D.M., Mancias, J.D., Mochida, G.H., Vagnoni, C.,
528 Johnson, J., Krogan, N., Harper, J.W., Reiter, J.F., et al. (2016). Microcephaly Proteins Wdr62
529 and Aspm Define a Mother Centriole Complex Regulating Centriole Biogenesis, Apical
530 Complex, and Cell Fate. Neuron *92*, 813–828.
531 Johnson, M.B., Wang, P.P., Atabay, K.D., Murphy, E.A., Doan, R.N., Hecht, J.L., and Walsh,
532 C.A. (2015). Single-cell analysis reveals transcriptional heterogeneity of neural progenitors in
533 human cortex. Nat. Neurosci. *18*, 637–646.
534 Johnson, M.B., Sun, X., Kodani, A., Borges-Monroy, R., Girskis, K.M., Ryu, S.C., Wang, P.P.,
535 Patel, K., Gonzalez, Di.M., Woo, Y.M., et al. (2018). Aspm knockout ferret reveals an
536 evolutionary mechanism governing cerebral cortical size. Nat. 2018 5567701 *556*, 370–375.
537 De Juan Romero, C., Bruder, C., Tomasello, U., Sanz-Anquela, J.M., and Borrell, V. (2015).

538 Discrete domains of gene expression in germinal layers distinguish the development of
539 gyrencephaly. EMBO J. *34*, 1859–1874.
540 Karasawa, S., Araki, T., Yamamoto-Hino, M., and Miyawaki, A. (2003). A Green-emitting
541 Fluorescent Protein from Galaxeidae Coral and Its Monomeric Version for Use in Fluorescent
542 Labeling. J. Biol. Chem. *278*, 34167–34171.
543 Kawasaki, H., Iwai, L., and Tanno, K. (2012). Rapid and efficient genetic manipulation of
544 gyrencephalic carnivores using in utero electroporation. Mol. Brain *5*, 1–7.
545 Kawaue, T., Shitamukai, A., Nagasaka, A., Tsunekawa, Y., Shinoda, T., Saito, K., Terada, R.,
546 Bilgic, M., Miyata, T., Matsuzaki, F., et al. (2019). Lzts1 controls both neuronal delamination
547 and outer radial glial-like cell generation during mammalian cerebral development. Nat.
548 Commun. 2019 101 *10*, 1–18.
549 Kessaris, N., Fogarty, M., Iannarelli, P., Grist, M., Wegner, M., and Richardson, W.D. (2005).
550 Competing waves of oligodendrocytes in the forebrain and postnatal elimination of an
551 embryonic lineage. Nat. Neurosci. 2005 92 *9*, 173–179.
552 Kou, Z., Wu, Q., Kou, X., Yin, C., Wang, H., Zuo, Z., Zhuo, Y., Chen, A., Gao, S., and Wang,
553 X. (2015). CRISPR/Cas9-mediated genome engineering of the ferret. Cell Res. 2015 2512 *25*,
554 1372–1375.
555 Liu, J., Liu, W., Yang, L., Wu, Q., Zhang, H., Fang, A., Li, L., Xu, X., Sun, L., Zhang, J., et al.
556 (2017). The Primate-Specific Gene TMEM14B Marks Outer Radial Glia Cells and Promotes
557 Cortical Expansion and Folding. Cell Stem Cell *21*, 635-649.e8.
558 McConnell, S.K. (1988). Fates of visual cortical neurons in the ferret after isochronic and
559 heterochronic transplantation. J. Neurosci. *8*, 945–974.
560 Noctor, S.C., Scholnicoff, N.J., and Juliano, S.L. (1997). Histogenesis of Ferret Somatosensory
561 Cortex. J. Comp. Neurol *387*, 179–193.
562 Nowakowski, T.J., Pollen, A.A., Sandoval-Espinosa, C., and Kriegstein, A.R. (2016).
563 Transformation of the Radial Glia Scaffold Demarcates Two Stages of Human Cerebral Cortex
564 Development. Neuron *91*, 1219–1227.
565 Nowakowski, T.J., Bhaduri, A., Pollen, A.A., Alvarado, B., Mostajo-Radji, M.A., Di Lullo, E.,
566 Haeussler, M., Sandoval-Espinosa, C., Liu, S.J., Velmeshev, D., et al. (2017). Spatiotemporal
567 gene expression trajectories reveal developmental hierarchies of the human cortex. Science
568 (80-.). *358*, 1318–1323.
569 Ohtsuka, T., Imayoshi, I., Shimojo, H., Nishi, E., Kageyama, R., and McConnell, S.K. (2006).
570 Visualization of embryonic neural stem cells using Hes promoters in transgenic mice. Mol.
571 Cell. Neurosci. *31*, 109–122.

572 Ortiz-Álvarez, G., Daclin, M., Shihavuddin, A., Lansade, P., Fortoul, A., Faucourt, M.,
573 Clavreul, S., Lalioti, M.E., Taraviras, S., Hippenmeyer, S., et al. (2019). Adult Neural Stem
574 Cells and Multiciliated Ependymal Cells Share a Common Lineage Regulated by the Geminin
575 Family Members. Neuron *102*, 159-172.e7.
576 Polioudakis, D., de la Torre-Ubieta, L., Langerman, J., Elkins, A.G., Shi, X., Stein, J.L., Vuong,
577 C.K., Nichterwitz, S., Gevorgian, M., Opland, C.K., et al. (2019). A Single-Cell
578 Transcriptomic Atlas of Human Neocortical Development during Mid-gestation. Neuron *103*,
579 785-801.e8.
580 Pollen, A.A., Nowakowski, T.J., Chen, J., Retallack, H., Sandoval-Espinosa, C., Nicholas, C.R.,
581 Shuga, J., Liu, S.J., Oldham, M.C., Diaz, A., et al. (2015). Molecular Identity of Human Outer
582 Radial Glia during Cortical Development. Cell *163*, 55–67.
583 Poluch, S., and Juliano, S.L. (2015). Fine-Tuning of Neurogenesis is Essential for the
584 Evolutionary Expansion of the Cerebral Cortex. Cereb. Cortex *25*, 346–364.
585 Pulvers, J.N., Bryk, J., Fish, J.L., Wilsch-Bräuninger, M., Arai, Y., Schreier, D., Naumann, R.,
586 Helppi, J., Habermann, B., Vogt, J., et al. (2010). Mutations in mouse Aspm (abnormal spindle-
587 like microcephaly associated) cause not only microcephaly but also major defects in the
588 germline. Proc. Natl. Acad. Sci. U. S. A. *107*, 16595–16600.
589 Qiu, X., Mao, Q., Tang, Y., Wang, L., Chawla, R., Pliner, H.A., and Trapnell, C. (2017).
590 Reversed graph embedding resolves complex single-cell trajectories. Nat. Methods *14*, 979–
591 982.
592 Rash, B.G., Duque, A., Morozov, Y.M., Arellano, J.I., Micali, N., and Rakic, P. (2019).
593 Gliogenesis in the outer subventricular zone promotes enlargement and gyrification of the
594 primate cerebrum. Proc. Natl. Acad. Sci. *116*, 7089 LP – 7094.
595 Reillo, I., and Borrell, V. (2012). Germinal Zones in the Developing Cerebral Cortex of Ferret:
596 Ontogeny, Cell Cycle Kinetics, and Diversity of Progenitors. Cereb. Cortex *22*, 2039–2054.
597 Reillo, I., De Juan Romero, C., García-Cabezas, M.Á., and Borrell, V. (2011). A role for
598 intermediate radial glia in the tangential expansion of the mammalian cerebral cortex. Cereb.
599 Cortex *21*, 1674–1694.
600 Rossi, A.M., Fernandes, V.M., and Desplan, C. (2017). Timing temporal transitions during
601 brain development. Curr. Opin. Neurobiol. *42*, 84–92.
602 Rowitch, D.H., and Kriegstein, A.R. (2010). Developmental genetics of vertebrate glial–cell
603 specification. Nat. 2010 4687321 *468*, 214–222.
604 Shitamukai, A., Konno, D., and Matsuzaki, F. (2011). Oblique radial glial divisions in the
605 developing mouse neocortex induce self-renewing progenitors outside the germinal zone that

606 resemble primate outer subventricular zone progenitors. J. Neurosci. *31*, 3683–3695.
607 Sidman, R.L., and Rakic, P. (1973). Neuronal migration, with special reference to developing
608 human brain: a review. Brain Res. *62*, 1–35.
609 Smart, I.H.M., Dehay, C., Giroud, P., Berland, M., and Kennedy, H. (2002). Unique
610 Morphological Features of the Proliferative Zones and Postmitotic Compartments of the Neural
611 Epithelium Giving Rise to Striate and Extrastriate Cortex in the Monkey. Cereb. Cortex *12*,
612 37–53.
613 Stuart, T., Butler, A., Hoffman, P., Hafemeister, C., Papalexi, E., Mauck, W.M., Hao, Y.,
614 Stoeckius, M., Smibert, P., and Satija, R. (2019). Comprehensive Integration of Single-Cell
615 Data. Cell *177*, 1888-1902.e21.
616 Szemes, M., Gyorgy, A., Paweletz, C., Dobi, A., and Agoston, D. V. (2006). Isolation and
617 characterization of SATB2, a novel AT-rich DNA binding protein expressed in development-
618 and cell-specific manner in the rat brain. Neurochem. Res. *31*, 237–246.
619 Trapnell, C., Cacchiarelli, D., Grimsby, J., Pokharel, P., Li, S., Morse, M., Lennon, N.J., Livak,
620 K.J., Mikkelsen, T.S., and Rinn, J.L. (2014). The dynamics and regulators of cell fate decisions
621 are revealed by pseudotemporal ordering of single cells. Nat. Biotechnol. 2014 324 *32*, 381–
622 386.
623 Tsunekawa, Y., Terhune, R.K., Fujita, I., Shitamukai, A., Suetsugu, T., and Matsuzaki, F.
624 (2016). Developing a de novo targeted knock-in method based on in utero electroporation into
625 the mammalian brain. Development *143*, 3216–3222.
626 Wang, X., Tsai, J.W., Lamonica, B., and Kriegstein, A.R. (2011). A new subtype of progenitor
627 cell in the mouse embryonic neocortex. Nat. Neurosci. *14*, 555–562.
628 Yamamoto, S., Yamashita, A., Arakaki, N., Nemoto, H., and Yamazaki, T. (2014). Prevention
629 of aberrant protein aggregation by anchoring the molecular chaperone αB-crystallin to the
630 endoplasmic reticulum. Biochem. Biophys. Res. Commun. *455*, 241–245.
631 Zheng, K., Wang, C., Yang, J., Huang, H., Zhao, X., Zhang, Z., and Qiu, M. (2018). Molecular
632 and Genetic Evidence for the PDGFRα-Independent Population of Oligodendrocyte Progenitor
633 Cells in the Developing Mouse Brain. J. Neurosci. *38*, 9505–9513.
634 Zhong, S., Zhang, S., Fan, X., Wu, Q., Yan, L., Dong, J., Zhang, H., Li, L., Sun, L., Pan, N.,
635 et al. (2018). A single-cell RNA-seq survey of the developmental landscape of the human
636 prefrontal cortex. Nature *555*, 524–528.
637

FIGURE TITLES AND LEGENDS

Figure 1. Temporal patterns of neurogenesis and gliogenesis in the cerebral cortex of ferrets

(A) Schematic of cortical development and emergence of neural progenitor diversity in humans and ferrets. Progenitors sequentially undergo DL-neurogenesis, UL-neurogenesis, and gliogenesis and form ependymal cells. In both humans and ferrets, RG and oRG have been morphologically and positionally identified while tRG have been reported in humans only. VZ, ventricular zone; ISVZ, inner subventricular zone; OSVZ, outer subventricular zone; IZ, intermediate zone; DL, deep layer; UL, upper layer; CP, cortical plate; Mn, migrating neuron; IP, intermediate progenitor; and EPC, ependymal cell. (B-G) Coronal sections of the somatosensory cortices immunostained for PAX6 (red), TBR2 (green), and OLIG2 (cyan) from early to late neurogenesis at E25, E32, E36, E40, P5, and P10. Scale bars: 100 μm. The position of image strips at each stage is shown in the dorsal hemisphere images presented below

Figure 2. Single-cell RNA-seq reveals ferret transcriptome signatures and the cell types

(A) Schematic illustration of the experimental design and time points to build the transcriptome atlas of developing somatosensory cortex of ferrets. Single cells were isolated using 10X Chromium (see STAR Methods). (B) UMAP visualization of cells colored by Seurat clusters and annotated by cell types (as shown in D, E). (C) UMAP plot of cells colored by samples. Labels were named by cell isolation stages with suffixes “AG” or “T” to indicate IUE samples with azamigreen or those with no IUE, respectively (See STAR Methods). RG, IP, OPC, and excitatory neuron populations are highlighted on the plot. (D) Heatmap showing expression profiles of cluster marker genes based on log fold-change values. Cells were grouped by Seurat clustering (transverse). Cell types were assigned according to the expression of marker and differentially expressed genes in each cluster; RG, radial glia; tRG, truncated RG; IPC, intermediate progenitor cell; DL, deep layer neurons; UL, upper layer neurons; OPC, oligodendrocyte precursor cell; ITN, interneuron; and EN, endothelial cells. Color bar matches Seurat clusters in (B). The representative genes among 10 topmost enriched genes are shown per cluster, with typical marker gene note on the right side. (E) Normalized expression levels of representative marker genes of different cell types projected onto the UMAP plot in (B). EP, ependymal and MG, microglia. (F) The expression pattern of *CRYAB*, a marker for tRG, which had been described only in humans and primates. (G) The expression pattern of *HOPX*, a marker for oRG in humans and primates in the UMAP plot. (H)Immunostaining for $CRYAB^{+}$

tRG (green) and HOPX$^+$ RG (red) together with DAPI on P1 and P10 germinal layers. HOPX$^+$ cells are observed in all germinal layers during late neurogenic stages

Figure 3. Comparison of molecular identity of RG subtypes between ferret and human

(A) UMAP visualization of integrated human (n=2672; left) and ferret (n=30, 234; right) single-cell dataset colored by different clusters. The names of clusters from human and ferret cells begin with "H" and "F" capitalization, respectively. (B) Proportional representation of cells from different stages and species. Schematics of the corresponding stages between ferrets and human are shown. (C, D) Correlation coefficient (C) and significance (D) between indicated clusters of ferrets and humans, calculated by marker gene scores. (E) Normalized expression levels of the indicated genes in humans and ferrets from each progenitor cluster. (F) tRG scores of the indicated cell in each cell cluster, presented as box-whiskers for humans and ferrets. The lines in the box-whiskers from top to bottom indicate maximum (except outliers), third to first quartile, median, and minimum (except outliers). The points outside the box indicate outliers. Outliers are 1.5-fold larger or smaller than interquartile range from the third or first quartile, respectively

Figure 4. Truncated tRG is emerged during postnatal cortical development in ferrets

(A) Representative image showing the cellular features of tRG in ferret P0 apical germinal zones stained for GFP and CRYAB. (B) Ferret embryonic RG was sparsely labelled with a GFP-expressing plasmid at E30 via IUE. MAX projection was performed on a 30 μm vibratome section with 5 μm interval for each z-image. Scale bar, 50 μm. (B) The expression patterns of CRYAB (green) and PAX6 (red) in ferret germinal zones during postnatal development (P1, P5, and P10). Cryosection thickness: 12 μm. (C) Quantification of CRYAB$^+$ cells among all nuclei (DAPI) in the VZ by immunohistochemistry (width, 150 μm; n=3 for P5; n=2 for P10; Wilcoxon rank-sum test *p*-value 6.574e-08). (D) Histogram showing the number of cells by age in the tRG cluster annotated in the ferret transcriptome dataset (Figure 2B). (E-G) Quantification of KI67-, TBR2-, or OLIG2-expressing cells among the CRYAB$^+$ cell population in the VZ (n=2 for P5; n=2 for P10 for each staining except n=3 for TBR2 staining), as displayed in the box and whisker plots. Box-whiskers indicate lines of the maximum and minimum, with a box of upper and lower quartiles with the median. (E'-G') Representative images with MAX projection used for quantification. Images were taken using a 100× objective lens with immersion oil on cortical slices of 12 μm (z-step, 1.5 μm). (H-M) Time-lapse imaging of EGFP-labeled progenitor cells forming tRG. Please refer to the text for

further details. EGFP fluorescence was visualized. The time below each snapshot strip indicates the time passed after the slice culture was started. (H-J) An apically attached IPC with a short basal fiber produced a tRG cell. (H) Sequential snapshots showing that an IPC formed tRG through apical division (both cells are marked in deep blue and by white arrows). The sibling cells of tRG are marked by bright blue color and open arrows. (I) Schematic representation of tRG formation recorded in (H). IPC and tRG are marked in deep blue; the sibling of tRG is indicated by light blue. (J) Immunostaining of a cryostat section from a fixed slice stained for Cryab (red) and EGFP (green). (K-L) A vRG cell is divided to produce an apical IPC that produces tRG. Please see the time-lapse movie 1 and main text for further details. (K) Sequential snapshots. The white arrowheads indicate ancestral vRG (pinked-colored); the white arrows (deep blue-colored cell body) indicate IPC generated from the vRG and then the CRYAB^{+} daughter of the IPC; open arrows indicate the other daughter of the divided IPC (light blue). (L) Schematic of time-lapse imaging, as shown in (K). (M) The cultured slice was fixed and stained for EGFP (green), CRYAB (red), and FOXJ1 (light blue). Scale bar, 50 µm

Figure 5. Temporal fates of RG cells predicted by pseudo-time trajectory analysis

(A) The pseudo-time trajectory branching tree of the developing cortex in ferrets (Monocle v2). Cellular distribution at each branch on UMAP plot shown in Figure 2B. Cell types representing each branch and their gene markers are shown next to the branches (see below). (B) Branching trees split by collection stages (AG samples are shown). (C) Distribution of cells expressing marker genes for major cell states or fates along trajectories. Color densities indicate the log-normalized unique molecular identifier (UMI) count for each gene. Branches strongly expressing Hes1 were named NPC 1, 2, and 3 branches. (D) The distribution of tRG cells along branching trees and tRG-focused UMAP visualization. The tRG cells (162) were found on three branches, NPC3 (9.3%; 15 cells), ependymal-tRG (61.1%; 99 cells), and astroglial-tRG (29.6%; 48 cells). (E) The composition of three types of tRG in (D) by the collection stage (AG and T samples are combined). No tRG cells were collected from E25 and E34

Figure 6. Ferret tRG undergo postnatal ependymal differentiation

(A) Immunostaining of 12-µm cortical cryosections for CRYAB (green) and FOXJ1 (red), focusing on the VZ at E40, P3, P5, P10, P14, and P35. Scale bar, 50 µm. (B) Numbers of FOXJ1-expressing cells in CRYAB-expressing cells in the VZ (n=3 for P5; n=2 for P10; Wilcoxon rank sum test *p*-value 1.749e-05). (C) Number of cells having UMI counts higher

than 0.25 for both *Cryab* and *Foxj1* in the mid and late RG, or tRG clusters is shown in Figure 2B. Color bars indicate the stages of sample collection. *Cryab*- and *Foxj1*-expressing cells increased over time in the tRG cluster only. (D) Normalized expression of *Foxj1* in the indicated ferret clusters. (E) Cortical origin and shape of FOXJ1-expressing ependymal cells. Staining for FOXJ1 at P14 after labeling cortical progenitors by an mCherry-expressing vector via IUE at E30. The maximum projection images with 1 μm z-step size are shown; cryosection thickness, 12 μm; scale bar, 20 μm. (F) The onset of ciliogenesis in the developing cortex of ferrets, as shown by staining for adenine cyclase III (cyan) along the VZ surface at E40, P5, P10, and P35. Scale bars, 10 μm

Figure 7. Comparison of tRG and oRG subtypes between ferrets and humans

(A) UMAP visualization of human brain cells colored by cell type and identified by marker genes (data from Bhaduri et al., 2021). (B) Schematic of the integration strategy of human and ferret subtypes. (C) UMAP visualization of integrated ferret and human datasets colored by different clusters. (D, E) Identification of three tRG subtypes in ferrets (D) and humans (E). The red dots highlight the indicated tRG subtypes. (F) Distribution of humans (left) and ferrets (right) tRGs in the integrated dataset. Human and ferret tRG were identified from the separated dataset. (G) Distribution of ferret tRG subtypes (identified by the pseudo-time analysis) in the integrated dataset. (H) Identification of oRG-like cells in ferret (left) and oRG in human (right). The red dots highlight the indicated oRG-like cells or oRGs. (I) oRG scores for oRG-like cells and other NPCs in ferrets. (J) The expression pattern of *CRYM*, CLU, and HOPX in oRG-like cells and other NPCs in ferrets. (F) *in situ* hybridization for *Clu* indicates that this gene is expressed in all of the VZ, ISVZ, and OSVZ.

762

763 **Supplementary Figure Legends**

764

765 **Figure S1. Development of the cerebral cortex in ferrets**

766 (A) Immunostaining for CTIP2 (green) and SATB2 (red) at the same developmental stages as
767 in Figure 1B, showing the onset of DL- (E25 or earlier) and UL-neurogenesis (E32-E34). VZ,
768 ventricular zone; ISVZ, inner subventricular zone; OSVZ: outer subventricular zone; IZ,
769 intermediate zone; DL, deep layer; UL, upper layer; and CP, cortical plate. Scale bars: 100 µm
770 (B) Gliogenic progenitors as revealed by immunostaining for GFAP in cortical germinal layers
771 at E32, E36, E40, P5, and P10. Scale bars: 100 µm
772 (C) Validation of cortically generated OLIG2^{+} oligodendrocyte precursors at P10 cerebral
773 cortex after mCherry labeling at E30. Arrowheads in the cropped images of the upper panels
774 (Figures S1C-i and S1C-ii) indicate cells that co-express mCherry, PAX6, and OLIG2 in the
775 OSVZ and VZ. Scale bars: 20 µm

776

777 **Figure S2. Cell types in the developing cerebral cortex of ferrets**

778 (A) Violin plots showing the number of genes (nFeature) and mRNAs (nCount) per cell in each
779 sample and time point. Progenitor clusters (mid RG, late RG, tRG, and IPC) contained more
780 cells from "AG" samples than from unsorted "T" samples, indicating a successful enrichment
781 of progenitor cell types in "AG" samples (Figure S2C). (B) Table comparing quality-control
782 metrics of an alignment with either MusPutFur 1.0 (UCSC gene models) or MusPutFur 2.60
783 (this study) using E34 samples. The total number of genes detected and median genes per cell
784 were higher with MusPutFur 2.60 (C) Heatmap of expression level of cell cycle marker genes
785 based on log fold-change values. *PCNA*, *DUT*, *SIVA1,* and *TYMS* are shown as markers of the
786 S-phase; *UBE2C*, *CDCA4*, *CENPF,* and *CCNB1* are shown as markers of the G2M-phase.
787 Three subclusters among early RG, late RG, and IPC clusters expressed different markers for
788 cell-cycle states. Color bar at top indicates seurat clusters matching those in Figure 2B. (D)
789 Dotplot showing average expression and percentage of expression of representative marker
790 genes for individual cell types in the merged dataset. The largest cluster was composed of
791 upper-layer neurons, and their four clusters were combined as a single "UL" group. P.E.,
792 percentage of expression and A.E., average expression. (E) Percentage of each cell type in the
793 merged dataset (left) and each sample (right). The color bar at the right matches samples of
794 cell collection in (A).

795

Figure S3 Comparison of molecular identity of RG subtypes between ferret and human

(A) UMAP visualization of integrated ferret (n=30, 234) and human (n=2672) single-cell datasets colored by different clusters. The names of clusters from human and ferret cells begin with "H" and "F", respectively. (B) Expression patterns of the indicated genes in each cluster. The color of the cycle indicates the expression level of each gene. The size of cycles indicates the percentage of cells expressing the gene in the indicated cluster

Figure S4. Emergence of ferret tRG during postnatal cortical development

(A) Cellular features of a tRG cell in cortex labelled with GFP at embryonic stages by IUE. Vibratome sections at P0 and P4 (thickness=200 μm) were immunostained for CRYAB (green) and GFP (red). CRYAB$^+$ truncated basal fibers spanned up to the SVZ. (B) CRYAB expression among RG subtypes with different morphology in P10 cortex. Percentage of CRYAB$^+$ cells in oRG (12 cells), vRG (15 cells), and tRG (12 cells), (n=3), distinguished by sparse labeling with GFP by electroporation at P1. Representative images below show that oRG cells do not express CRYAB. (C) Pies showing the percentage of *Cryab* expression in the ferret clusters of the transcriptome dataset (Figure 2). Cells were counted positive if log-normalized UMI counts for *Cryab* were higher than 0.25 using Seurat "WhichCells" function (slot="data"). (D) Violin plot indicating the normalized expression of *Cryab* in ferret clusters shown in Figure 2. (E) Numbers of *Cryab*-expressing cells in the transcriptome dataset (Figure 2). *Cryab* expression was undetectable at E25. *Cryab*-expressing cells in the midRG and lateRG subtypes did not change in all stages (cell numbers; 58, 46, 68, 55, and 61 at E34, E40, P1, P5, and P10, respectively), while the number of *Cryab*$^+$ tRG cells increased after birth (cell numbers; 0, 21, 50, 91, and 118 at E34, E40, P1, P5, and P10, respectively). (F) The onset of CRYAB expression on the germinal layers of developing cortex in ferrets. Immunostaining for CRYAB (left) and DAPI (right) on cryosections at E32, E40, P3, P5, and P10 (thickness=12 μm). (G) Violin plots indicating the normalized expression levels of *Tbr2* (or *Eomes*) and *Olig2* in ferret clusters shown in Figure 2. (H) Gene enrichment analysis using tRG markers on EnrichR (572 genes found by FindMarkers Seurat function; X-axis, -log10 (adjusted *p-value*). Biological processes are shown (-LOG10 (adjusted *p-value*)>2.25) (I) To determine the appropriate timing of time-lapse observation (Figure 4H, I), a late timing of divisions of progenitors producing tRG was examined by labelling cells with EdU at E30 (producing deep layer neurons), E34 (Layer IV), E38 (upper layer neurons), and P6 (late neurogenic stages), and chasing labelled cells at P35.

Figure S5. Temporal fates of RG cells identified by pseudo-time trajectory analysis

(A) Ferret cells used for pseudo-time trajectory analysis were lined up along the stretched pseudo-time axis. These cells were color-coded according to collection (orig.ident) and UMAP clusters (Subtype.combined), separately. Along the pseudo-time axis, expression levels of marker-genes are also shown for typical cell types; LIX1 and HMGA2 for early RG, EOMES and NEUROG2 for IP, RGS20, and PTN for late RG, PDGFR and OLIG2 for glial cells, and FOXJ1 and FAM216B for ependymal cells. (B) Branching trees labelled by pseudo-time score. Color scale indicates log10 (pseudo-time +0.1) values. Each branch is named after the major cell type or state. (C) The composition of each branch by clusters is shown in the UMAP plot (Figure 2). Percentage was calculated for a cluster among all cells from a branch. (D) Branching trees split by UMAP clusters (Figure 2).

Figure S6. Comparison of the tRG and oRG subtypes between ferrets and humans

(A, B) A matrix of correlations between two arbitrary RG subtypes from humans and ferrets by calculating marker gene scores as described for Figure 3. (A) Correlations and (B) *p*-values between pairs in human and ferret clusters are shown (see STAR Methods). The early RG in ferrets showed the highest similarity with "OLIG1" in human data (see Figure S7B and its legend). This might be because of two reasons; (1) we included human cells from GW25 only and no human early RG in this dataset, and (2) cells in "OLIG1" highly expressed genes related with cell proliferation, which was observed in the early RG also (added to the supplementary table S4). We did not observe any cell types in human data corresponding to the ferret "midRG" with the same reason described above. (C) Distribution of human and ferret tRGs in the integrated dataset. The number in the X-axis indicates the cluster number identified by the UMAP in Figure 7C. (D) Expression pattern of the subtype maker genes in the three tRG-enriched clusters (7, 21, and 28). (E) The expression patterns of *CRYM*, CLU, and HOPX in oRG-like cells and other NPCs in humans. (F) *in situ* hybridization of *Clu* at the ferret cortex showed its expression in all of the VZ, ISVZ, and OSVZ at P5.

Figure.1. Development of the ferret cerebral cortex.

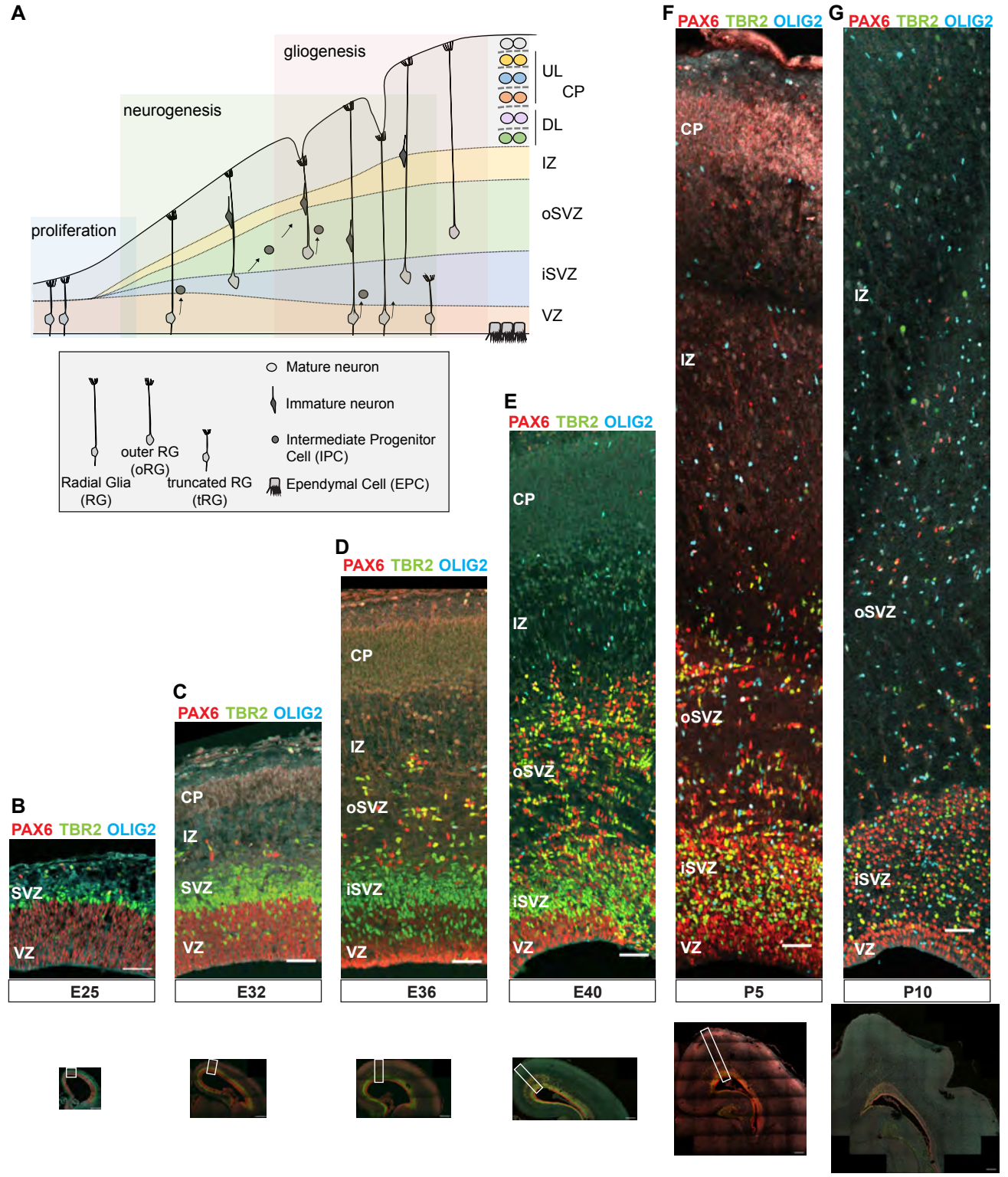

Figure S1. Development of the ferret cerebral cortex.

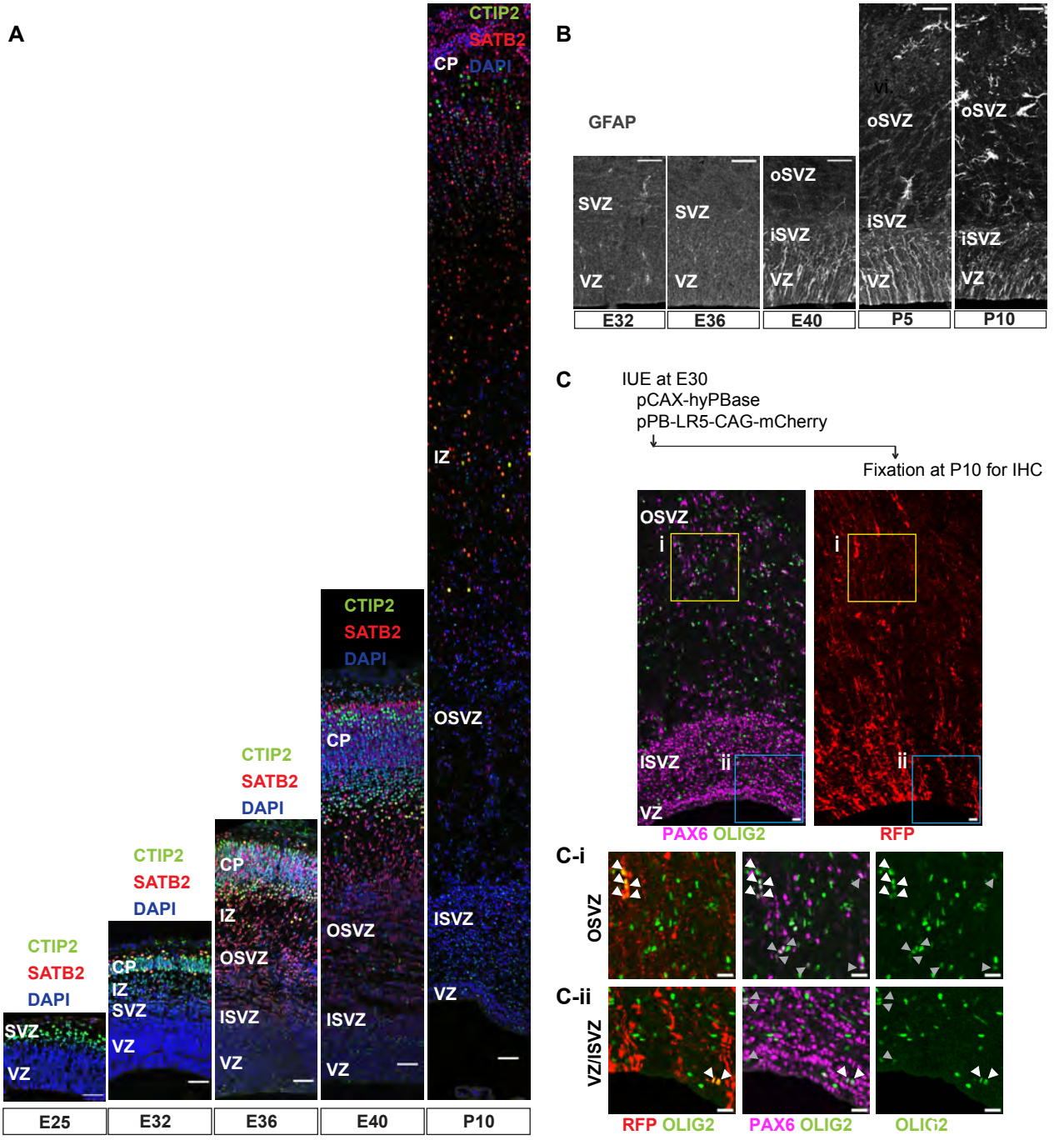

Figure.2. Cell types in developing ferret cerebral cortex.

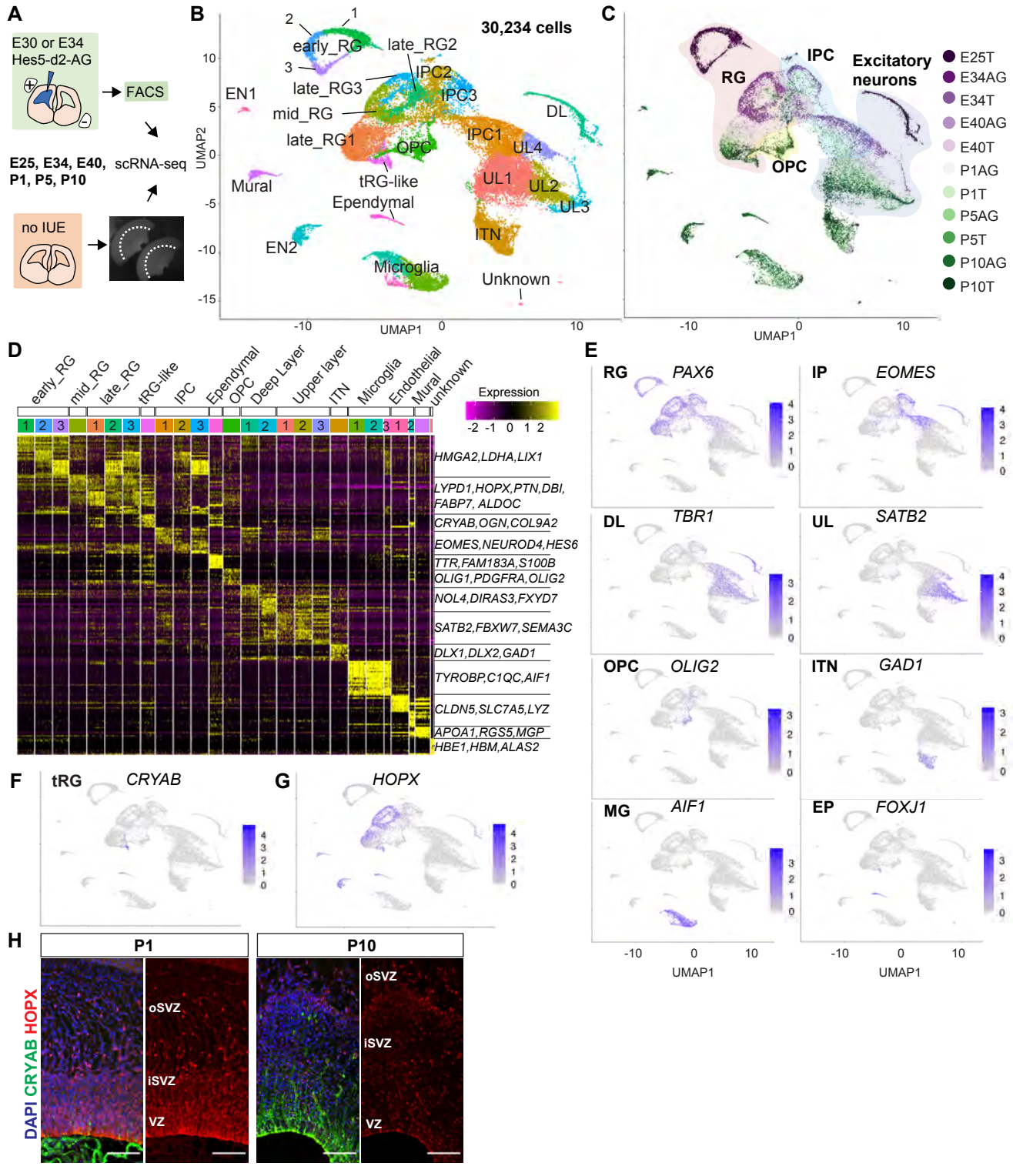

Figure S2. Cell types in developing ferret cerebral cortex.

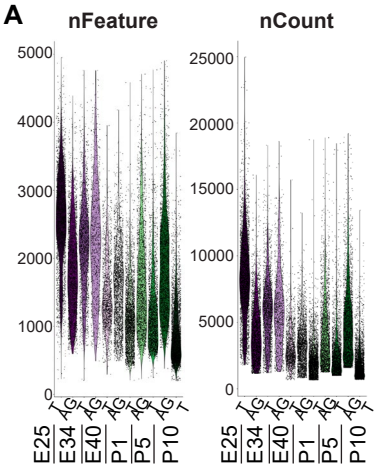

B

	Reference	Estimated Number of Cells	Median Genes per Cell	Number of Reads	Reads Mapped to Transcriptome	Total Genes Detecte	Median UMI Counts
E34_AG	NCBI	3,226	953	137673935	30.70%	14,562	2,153
E34_AG	This study	3,223	1,763	137,673,935	58.20%	17,886	3,983
E34_T	NCBI	2,260	1,182	107508876	29.90%	14,445	3,096
E34_T	This study	2,265	2,195	107,508,876	56.40%	17,838	5,863

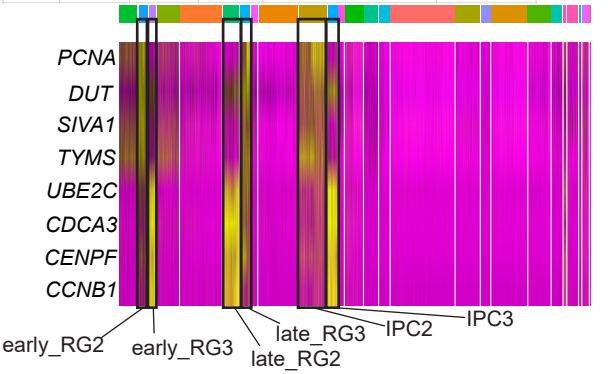

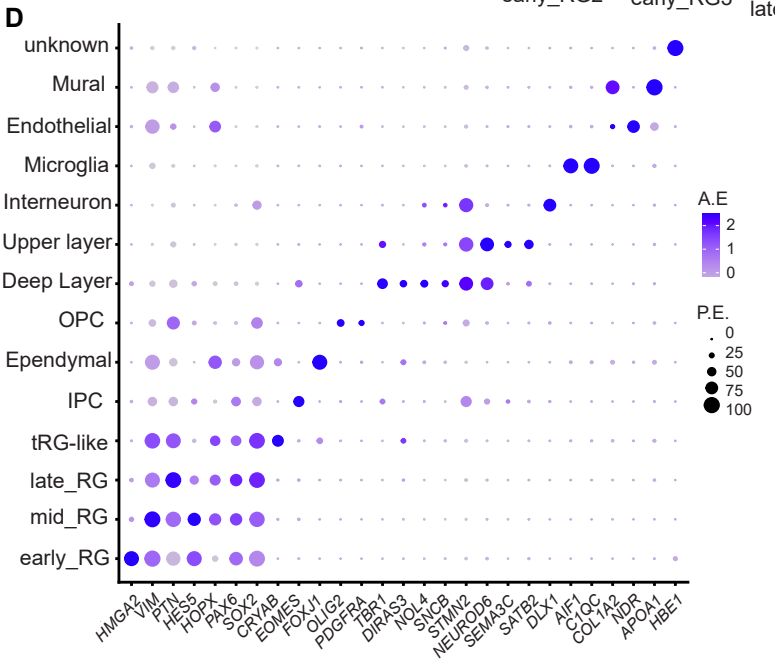

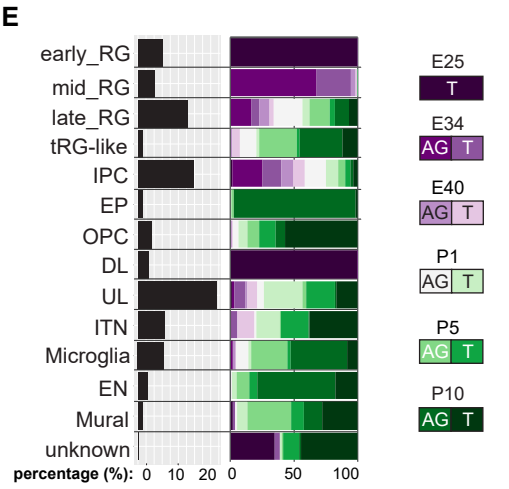

Figure 3. Comparison of molecular identity of RG subtypes between ferret and human.

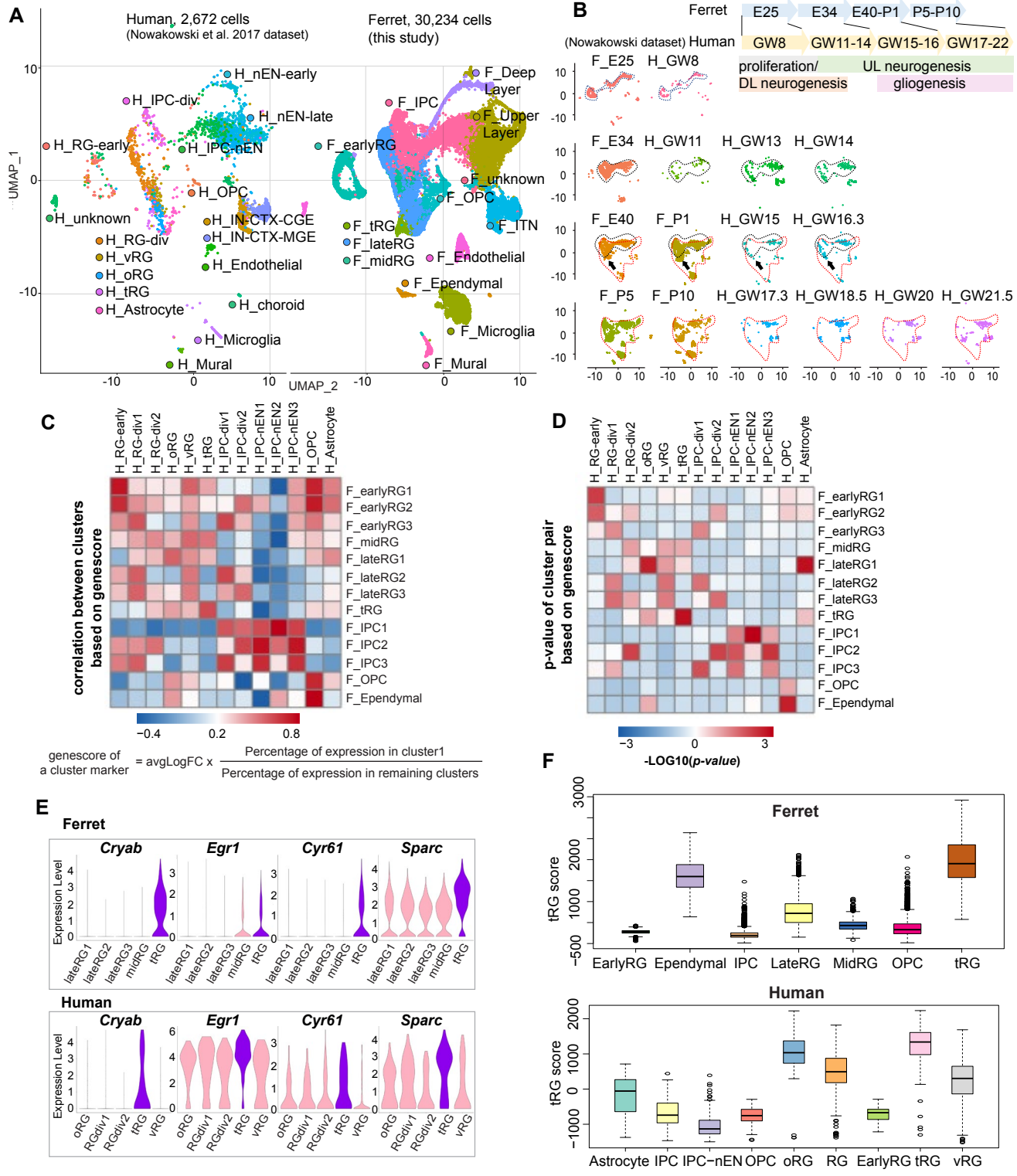

Figure S3. Comparison of molecular identity of RG subtypes between ferret and human.

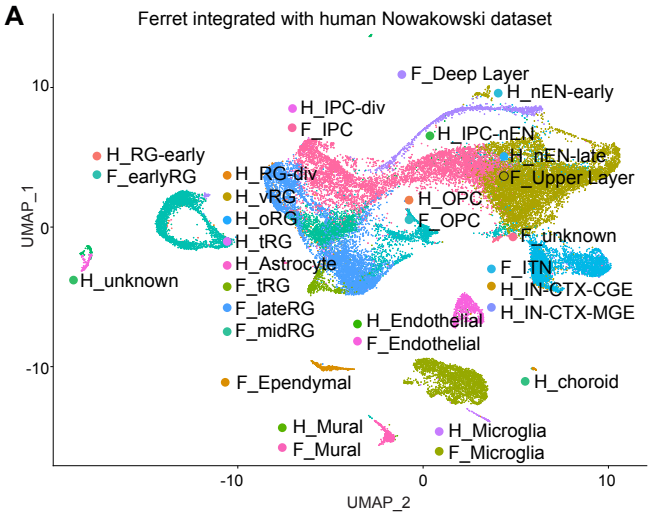

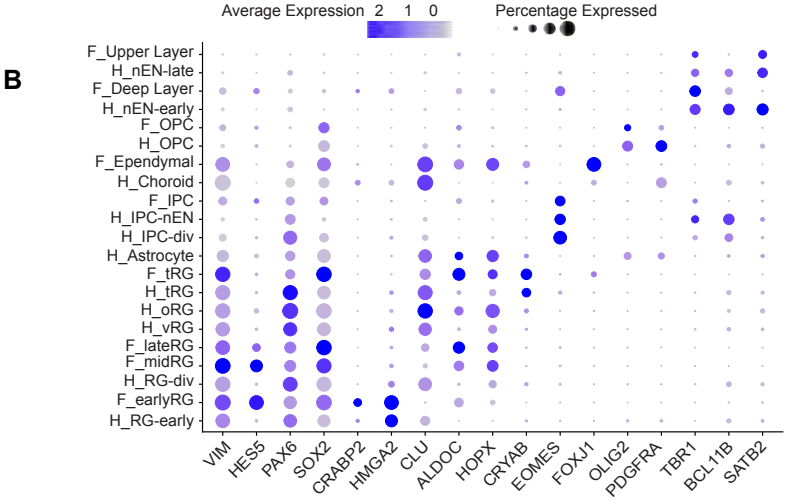

Figure 4. Emergence of ferret tRG during post-natal cortical development.

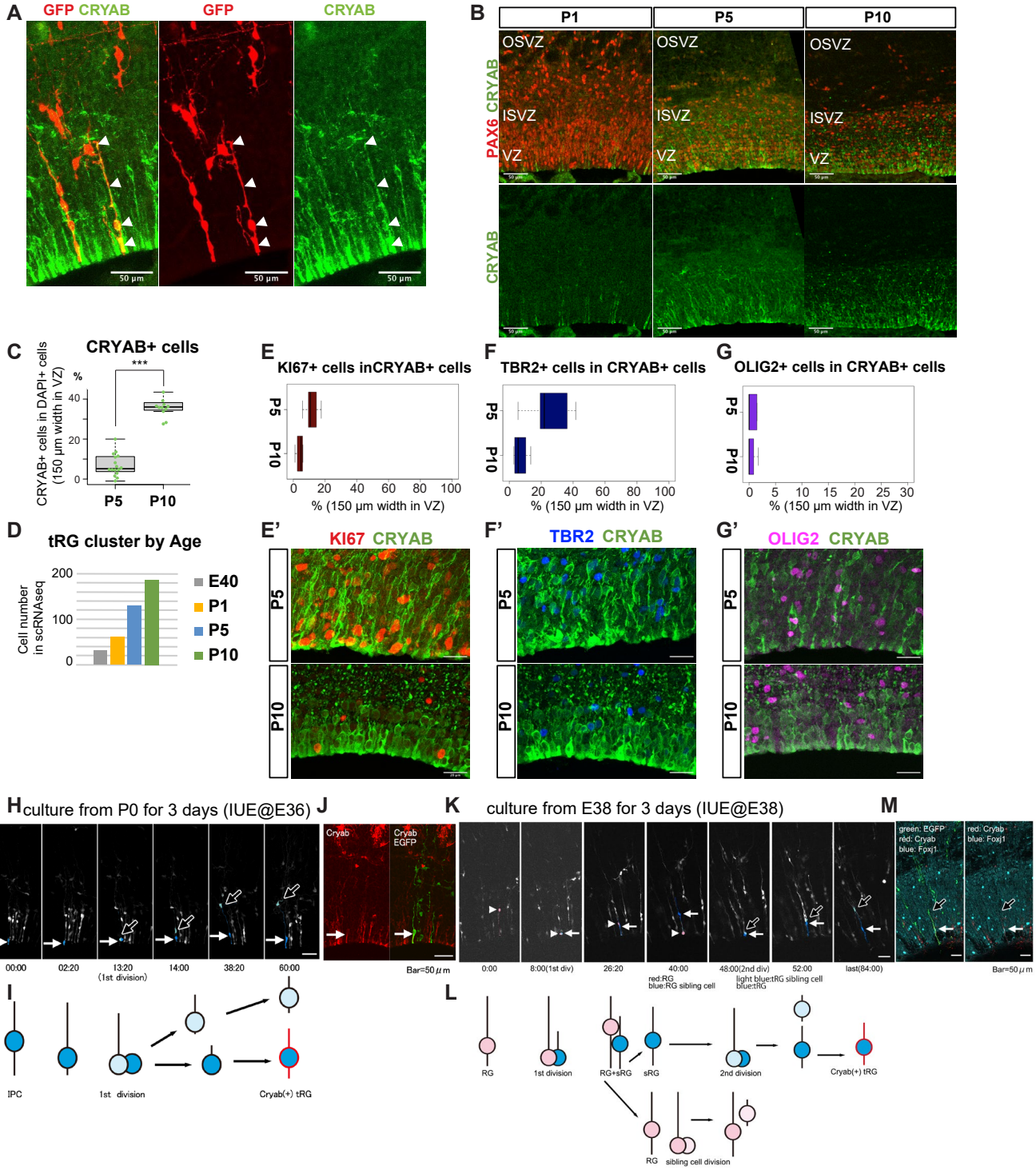

Figure S4. Emergence of ferret tRG during post-natal cortical development.

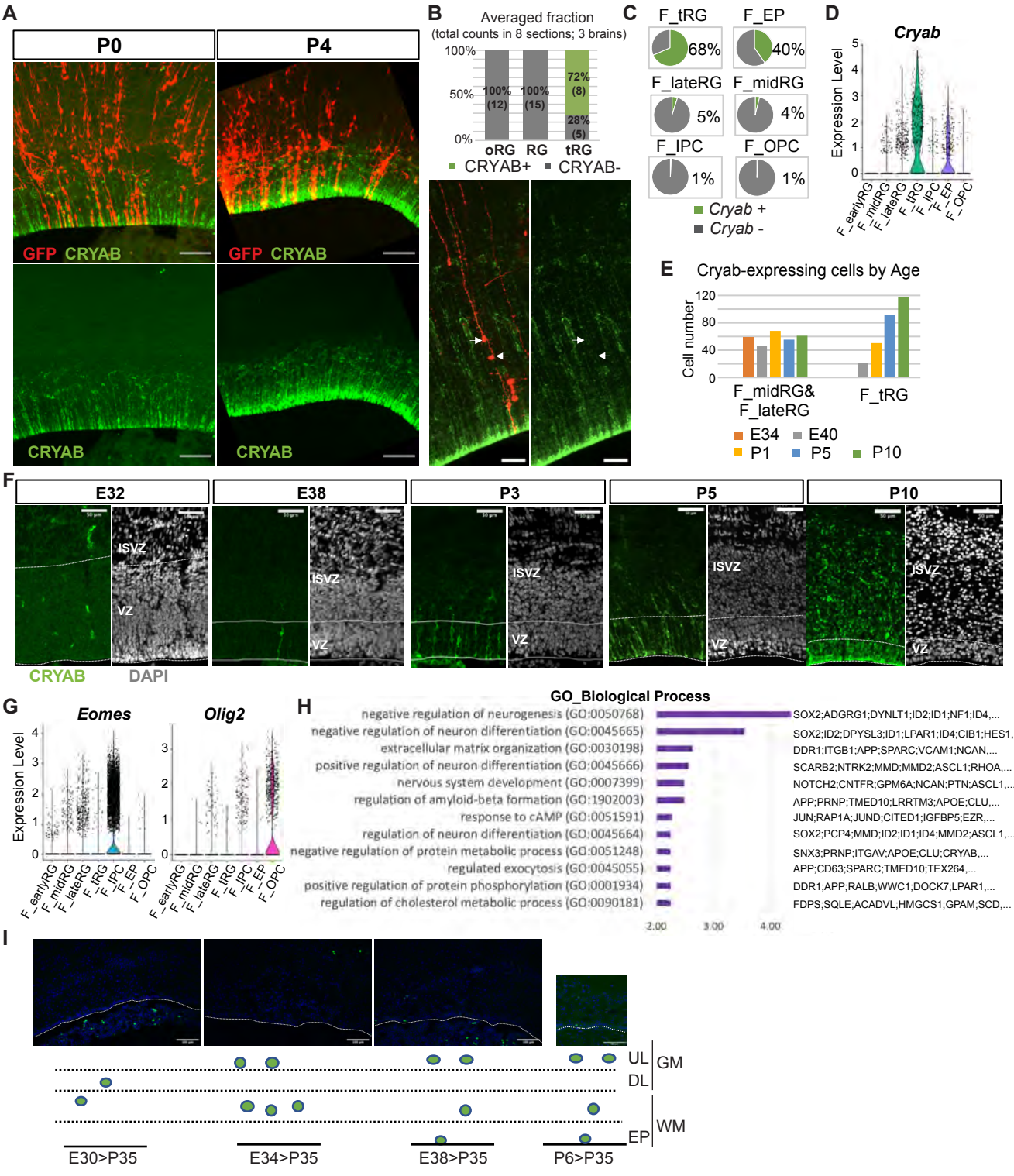

Figure 5. tRG contribute to ependymal and glial production.

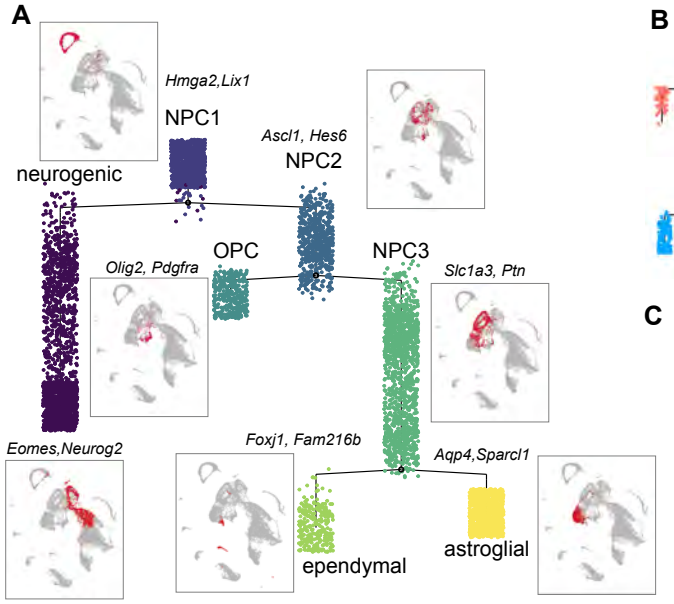

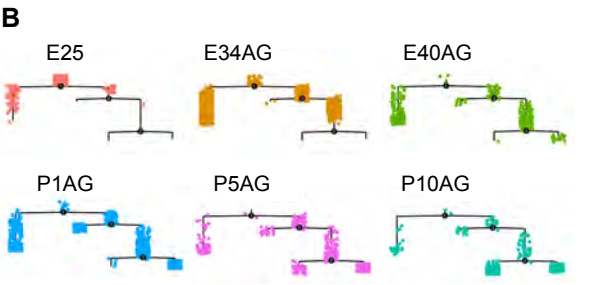

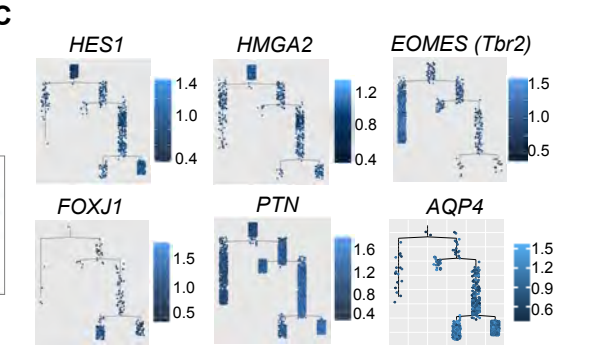

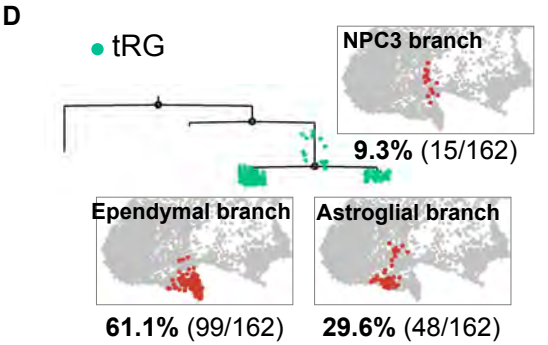

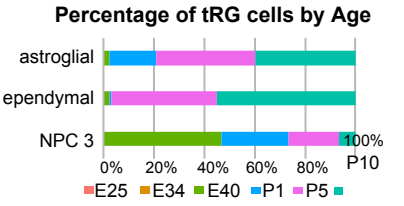

Figure S5. tRG contribute to ependymal and glial production.

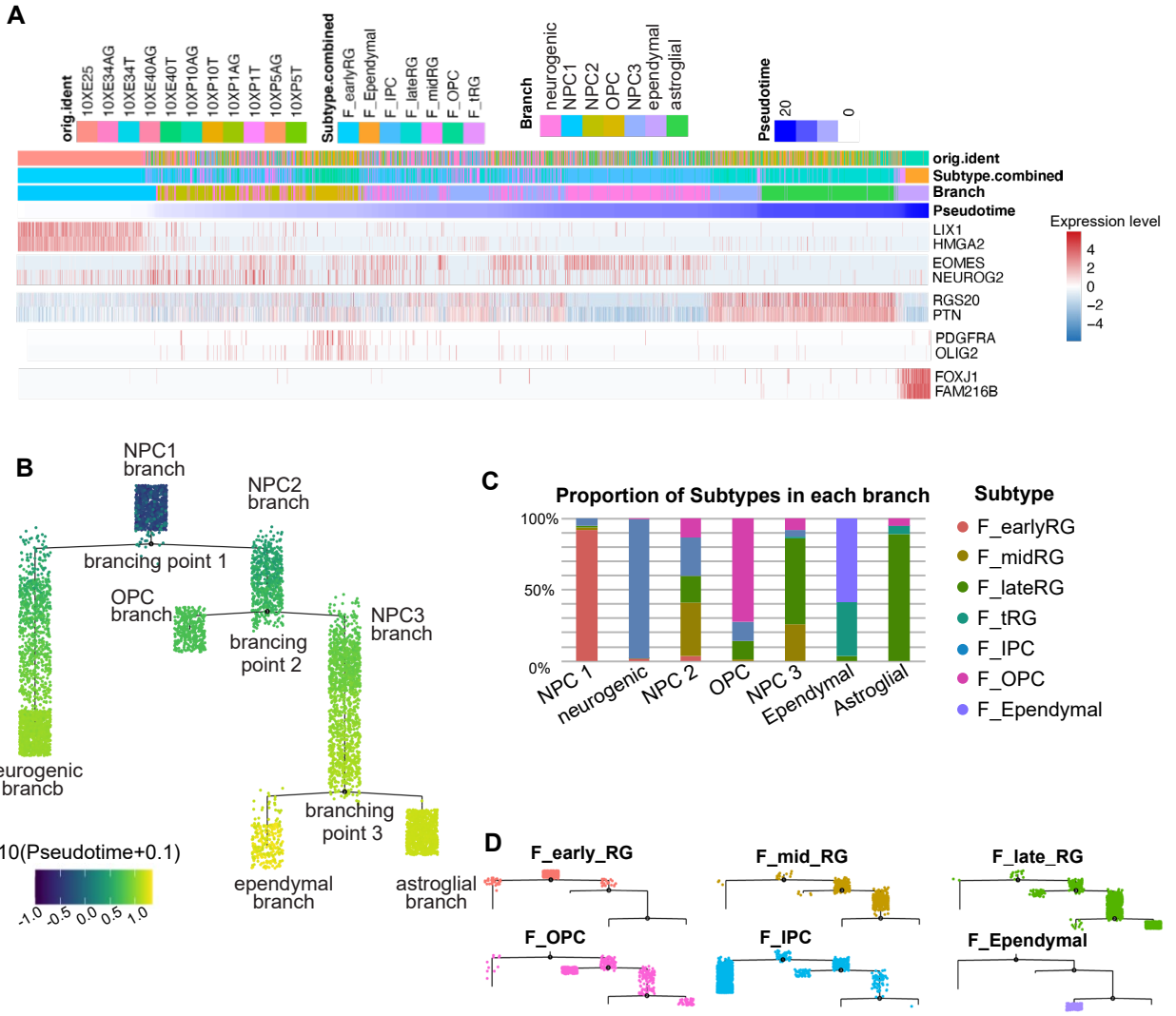

Figure.6. Ferret tRG undergo ependymal differentiation postnately in ferrets.

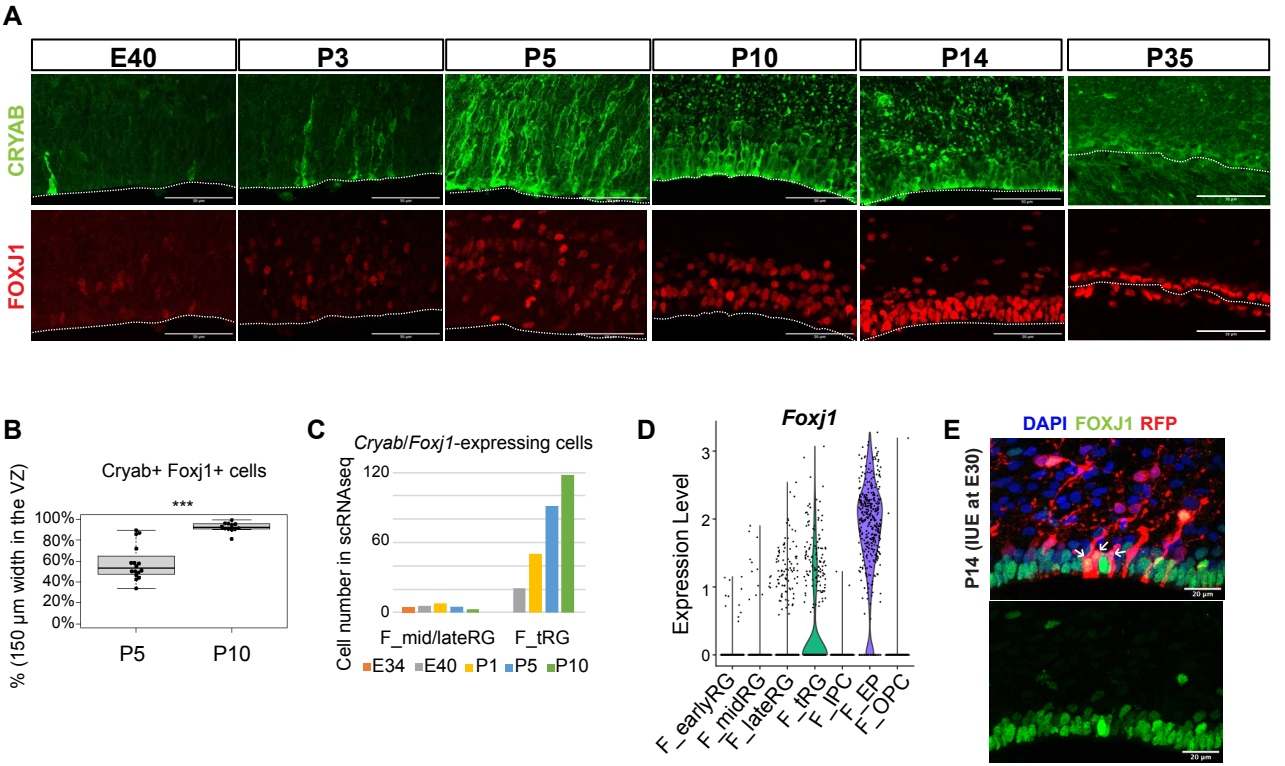

Figure 7 . Comparison of diffrential tRG states between ferret and human.

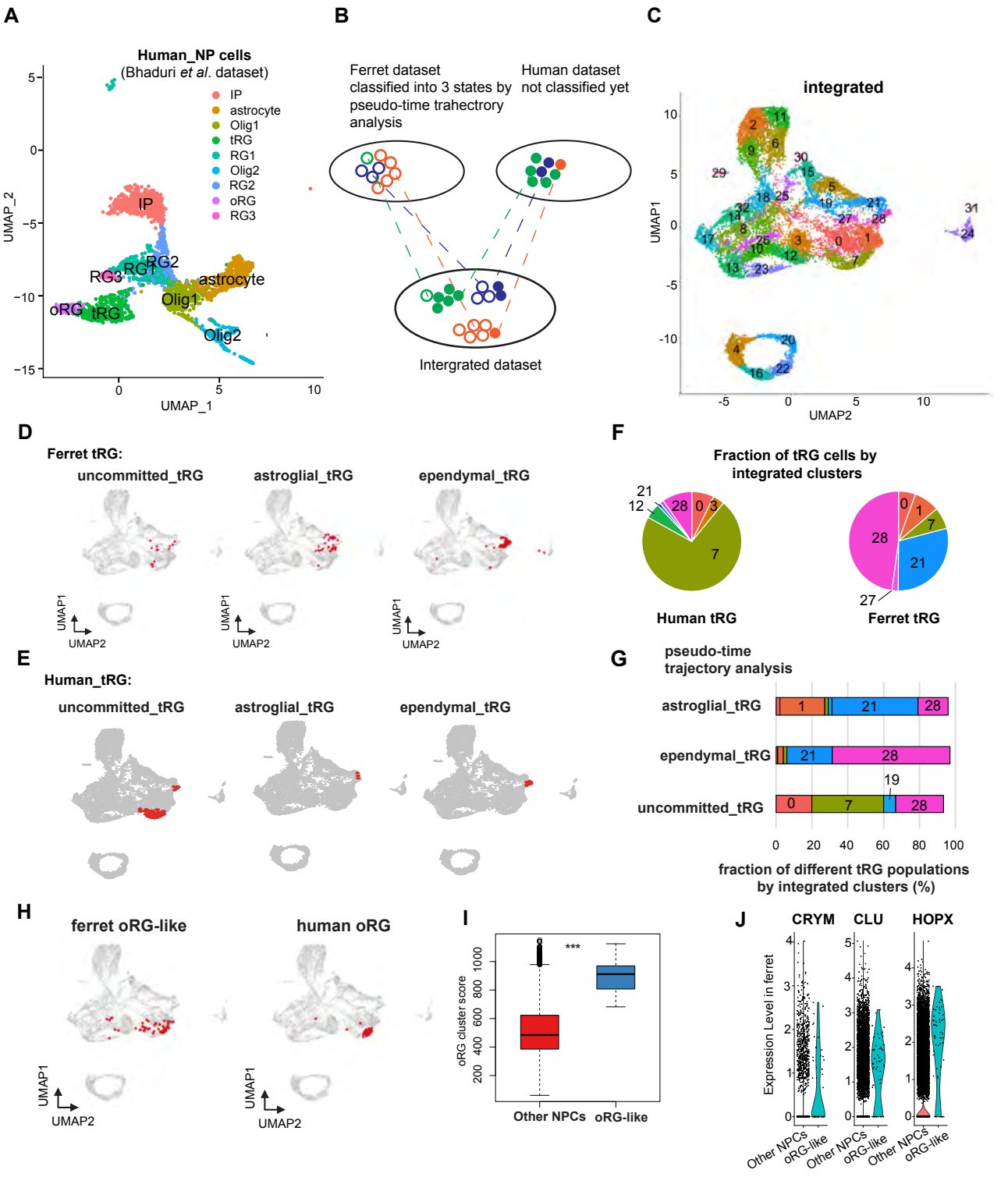

Figure S6 . Comparison of differential tRG states between ferret and human.